Lyapunov exponents of multi-state cellular automata

M. Vispoel,[1] A. J. Daly,[1] and J. M. Baetens[1]

Department of Data Analysis and Mathematical Modelling, Ghent University, Ghent, 9000, Belgium.

(*Electronic mail: milan.vispoel@ugent.be.)

(Dated: 14 March 2023)

In order to describe the sensitivity of a cellular automaton (CA) to a small change in its initial configuration, one can attempt to extend the notion of Lyapunov exponents as defined for continuous dynamical systems, to CA. So far, such attempts have been limited to CA with two states. This poses a significant limitation on their applicability, as many CA-based models rely on three or more states. In this paper, we generalize the existing approach to arbitrary N-dimensional k-state CA with either a deterministic or probabilistic update rule. Our proposed extension establishes a distinction between different kinds of defects that can propagate, as well as the direction in which they propagate. Furthermore, in order to arrive at a comprehensive insight into a CA's stability, we introduce additional concepts such as the average Lyapunov exponent and the correlation coefficient of the difference pattern growth. We illustrate our approach for some interesting three-state and four-state rules, as well as a CA-based forest fire model. In addition to making the existing methods generally applicable, our extension make it possible to identify some behavioral features that allows us to distinguish class IV CA from class III CA (according to Wolfram's classification), which has been proven to be difficult.

There have been many attempts to define Lyapunov exponents in the framework of cellular automata (CA)[1,4,8,24,26,30]. However, these approaches are limited to one-dimensional and/or two-state CA. In this paper, we propose an approach that is applicable to CA of any dimension and with any number of states. We define a single Lyapunov profile for every possible type of defect. We illustrate the usefulness of such profiles by using them as the basis for a behavioral analysis of three-state totalistic CA over the four different Wolfram behavioral classes. Finally we use the average Lyapunov exponents to study the stability of a probabilistic CA-based forest fire model.

I. INTRODUCTION

Many different measures have been proposed to describe and quantify the behavior of CA. Generally they can be categorized as either rule-table parameters or space-time parameters[6,9,14,29–31]. The former are derived from the CA's rule table and are often called genotypic parameters. The Langton parameter is a well-known example of this parameter type[14]. The space-time parameters are based on an inspection of the space–time patterns generated by the CA and are often called phenotypic parameters. Well-known examples include the entropy[30] and Kolmogorov complexity[9] of the space-time patterns. A useful parameter that captures a CA's sensitive dependence on the initial configuration and yields insight into its possible chaotic dynamics is its Lyapunov exponent. Computing the Lyapunov exponent of a CA requires knowledge of the difference pattern as well as the Boolean derivatives of the rule table, which essentially makes it a hybrid parameter with characteristics of both a rule table and a space-time parameter.

The Lyapunov exponent of a dynamical system is a measure of the rate of separation of two trajectories that are infinitesimally close in phase space[10,20,27]. As such, the Lyapunov exponent tells you if a dynamical system is stable in response to a perturbation of its initial condition. For an N-dimensional dynamical system, the rate of separation will depend on the orientation of the initial separation vector in phase space. This yields a spectrum of N Lyapunov exponents, one for each direction in phase space. As soon as one Lyapunov exponent in the spectrum is non-zero, any perturbation to the initial condition grows exponentially over time.

However, it is not straightforward to define Lyapunov exponents in the framework of CA as their

original definition relies on the tools of differential calculus, which are not available in the framework of CA where time, space and the state space are discrete. For one-dimensional binary CA, there are two options regarding a formal definition. The first definition, suggested by Wolfram[30], defines the directional Lyapunov exponent empirically as the average speed with which the difference pattern propagates to the left or right. Shereshevsky[24] later formalized this approach, which was further refined by other authors[8,26].

The second definition was proposed by Bagnoli *et al.*[2–4]. The (Hamming) distance between two initially nearby configurations in phase space can grow at most linearly with time due to the local nature of CA. In order to arrive to the familiar notion of Lyapunov exponents as the exponential divergence rate of nearby trajectories[10], Bagnoli *et al.*[4] considered the number of possible defect paths that arrive at a certain cell instead of merely the absolute difference of the original and perturbed values at a certain cell. Baetens *et al.*[1] refined this approach in order to yield the full Lyapunov profile of the CA.

Both definitions are only applicable to binary CA, which places an important limit on their usefulness is in practical scenarios since many CA-based models require three or more states. Examples thereof include disease spread models requiring susceptible, infected and recovered states[21], excitable media models requiring excitable, excited and refractory states[16,22], and forest-fire models requiring fuel, burning, empty and burnt states[17].

Motivated by this shortcoming, in this paper we demonstrate how Bagnoli's[4] approach for binary CA can be extended to k-state CA by explicitly accounting for the directionality of the defects, which means that a state change from a to b is not the same as a state change from b to a. In addition to generalizing the existing framework, this extension provides insights into the different types of defects that dominate the chaotic regime of a certain CA rule.

Section II B provides a recap of Lyapunov profiles in the context of two-state CA. Section II D extends the approach to multi-state CA and provides an illustrative example in the form of the totalistic three-state rule 420. Our results are described in Section III. Section III B describes the Lyapunov profiles over the different Wolfram classes, Section III C discusses some average Lyapunov exponents for four-state rules, Section III D illustrates the usefulness of the difference pattern growth plot and Section IV shows how our approach can be applied to a CA-based forest fire model. Finally, our conclusions are presented in Section V

II. LYAPUNOV PROFILES OF CELLULAR AUTOMATA

A. Preliminaries

A CA can be conveniently represented by a sextuple $\mathscr{C} = \langle \mathscr{T}, S, s, s_0, \mathscr{N}, \phi \rangle$. Here, $\mathscr{T}$ denotes a countably infinite tessellation of a one-dimensional Euclidean space, consisting of consecutive intervals $c_i, i \in \mathbb{N}$, referred to as cells, and S constitutes the space of states of the CA. The output function $s : \mathscr{T} \times \mathbb{N} \to S$ yields the state value of cell c_i at the t-th discrete time step, i.e. $s(c_i,t)$. The function $s_0 : \mathscr{T} \to S$ assigns to every cell c_i an initial state, i.e. $s(c_i,0) = s_0(c_i)$. $\mathscr{N}(c_i)$ is the neighborhood function with size $|\mathscr{N}|$, i.e. $\mathscr{N}(c_i) = (c_{i-1}, c_i, c_{i+1})$ in the case of nearest neighbors. Finally, the transition function $\phi : S^{|\mathscr{N}|} \to S$, that governs the dynamics of each cell c_i, is given by

$$s(c_i,t+1) = \phi(s(c_{i-1},t), s(c_i,t), s(c_{i+1},t)) .$$

The most basic CA have $|S| = 2$ and $|\mathscr{N}| = 3$. Such CA are called elementary CA (ECA). Another important class of CA are totalistic CA. For totalistic rules, the state space is endowed with the regular addition, and the updated cell value depends only on the sum of the values in its neighborhood at the previous time step, or mathematically: $s(c_i,t+1) = \phi(s(c_{i-1},t) + s(c_i,t) + s(c_{i+1},t))$.

Based on a visual inspection of the space-time patterns that a CA tends to generate, we can classify every CA into one of Wolfram's four behavioral classes: Class I (fixed point behavior), Class II (periodic behavior), Class III (chaotic behavior) and Class IV (complex behavior).

The next section provides an overview of the approach by Bagnoli *et al.*[4] to retrieve the Lyapunov exponents of two-state CA, after which we generalize this approach to CA with an arbitrary number of states.

B. Two-state CA: methodology

The space-time pattern generated by a CA rule can be interepreted as a trajectory in the CA configuration space $S^{\mathbb{N}}$. However, since CA are fully discrete, there is no notion of infinitesimally close configurations. Instead, we will consider initial configurations that differ at a single cell. The difference pattern $\Delta s(t)$ indicates how such a perturbation in the initial configuration, referred to

as a defect, propagates to subsequent time steps

$$\Delta \boldsymbol{s}(t+1) = \boldsymbol{s}(t) - \boldsymbol{s}^*(t)\,, \tag{1}$$

where subtraction occurs modulo 2, $\boldsymbol{s}(t)$ is the original space-time pattern and $\boldsymbol{s}^*(t)$ the perturbed space-time pattern obtained by perturbing the value of a single cell in the initial configuration of the original space-time pattern. For one-dimensional binary CA, we can use the Boolean Jacobian matrix $\boldsymbol{J}(\boldsymbol{s}(t),t)$ to obtain an update equation for the time evolution of the difference pattern:

$$\Delta \boldsymbol{s}(t+1) = \boldsymbol{J}(\boldsymbol{s}(t),t) * \Delta \boldsymbol{s}(t)\,, \tag{2}$$

where $*$ denotes the usual matrix multiplication but with the regular summation replaced by summation modulo 2[4]. The matrix $\boldsymbol{J}(\boldsymbol{s}(t),t)$ in Eq. (2) contains the Boolean partial derivatives[28] of the transition function $\phi : S^{|\mathscr{N}|} \to S$:

$$\left[\boldsymbol{J}(\boldsymbol{s}(t),t)\right]_{ij} = \frac{\partial s(c_i,t+1)}{\partial s(c_j,t)} \tag{3}$$

$$= \begin{cases} 1, & \text{if } \phi\left(\tilde{s}(\mathscr{N}(c_i),t)\right) \neq \phi\left(\tilde{s}_j(\mathscr{N}(c_i),t)\right), \\ 0, & \text{otherwise,} \end{cases} \tag{4}$$

where $\tilde{s}_j(\mathscr{N}(c_i),t)$ is the tuple obtained by replacing $s(c_j,t)$ by its complement in the tuple $\tilde{s}(\mathscr{N}(c_i),t)$.

The Jacobian's elements simply indicate whether or not flipping the value at cell c_j at time t causes a change in the value at cell c_i at time $t+1$. Whether or not a change at cell c_j propagates to cell c_i depends on its neighborhood $\mathscr{N}(c_i)$, which is why $\boldsymbol{J}(\boldsymbol{s}(t),t)$ depends on the configuration $\boldsymbol{s}(t)$. As such, the entries of $\boldsymbol{J}(\boldsymbol{s}(t),t)$ reflect the local stability of the CA at time step t[23]. Note that for one-dimensional CA with a neighborhood consisting of nearest neighbors only, $\boldsymbol{J}(\boldsymbol{s}(t),t)$ is a tridiagonal matrix since the right hand side of Eq. (4) vanishes when $c_j \notin \mathscr{N}(c_i)$.

In order to define Lyapunov exponents, we need to be able to define an exponential divergence of nearby trajectories in the CA configuration space. The most straightforward choice of a metric to obtain such a divergence, is the Hamming distance d_h. The Hamming distance between the original and perturbed space-time pattern at a certain time step $H(t)$ is given by the sum of all the elements

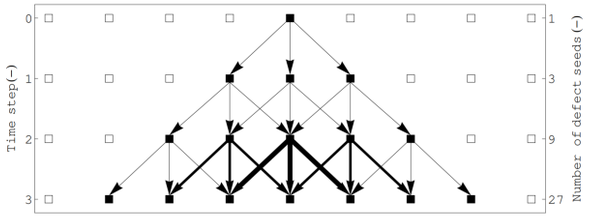

FIG. 1: Defect pattern when a single defect is introduced at the center of a two-state CA, with arrows indicating all possible ways defects can propagate. Reproduced with permission from Journal of Cellular Automata 13, (2015). Copyright 2015 Old City Publishing.

of the difference pattern at that time step

$$H(t) = d_h(\boldsymbol{s}(t), \boldsymbol{s}^*(t)) \tag{5}$$

$$= \sum_i \Delta s(c_i, t). \tag{6}$$

However, due to the local nature of CA dynamics, $H(t)$ can grow at most linearly with time

$$H(t) \leq 2t + 1, \tag{7}$$

so we cannot use the Hamming distance when we aim to define an exponential divergence of trajectories in $S^{\mathbb{N}}$. To allow for such a divergence, we may instead consider the number of ways in which defects can propagate to the t-th row of the difference pattern, instead of simply considering the number of defects at a certain cell up to a given time step[4]. This is indicated by the arrows in Figure 1. Let $\boldsymbol{d}(t)$ be the defect pattern whose i-th element is the number of ways in which the initial defect can propagate to cell c_i after t time steps. Again we may use the Boolean Jacobian matrix $\boldsymbol{J}(\boldsymbol{s}(t), t)$ to obtain an update equation for the time evolution of the defect pattern

$$\boldsymbol{d}(t+1) = \boldsymbol{J}(\boldsymbol{s}(t), t)\boldsymbol{d}(t)\,, \tag{8}$$

where regular matrix multiplication and summation take place. The sum of the elements of the defect pattern equals the total number of ways in which defects can propagate to the t-th row of the difference pattern $D(t) = \sum_i d_i(t)$. $D(t)$ can grow exponentially with time, allowing us to arrive at a definition of a Lyapunov exponent that complies with their original definition in the theory of dynamical systems[10].

In summary, for one-dimensional binary CA the time evolution of the difference pattern $\boldsymbol{s}(t)$ and defect pattern $\boldsymbol{d}(t)$ is governed by the following update equations:

$$\Delta\boldsymbol{s}(t+1) = \boldsymbol{J}(\boldsymbol{s}(t),t) * \Delta\boldsymbol{s}(t), \tag{9}$$

$$\boldsymbol{d}(t+1) = \boldsymbol{J}(\boldsymbol{s}(t),t)\boldsymbol{d}(t). \tag{10}$$

From Eq. (9) we may infer the upper bounds for $H(t)$ and $D(t)$[1]:

$$H(t) = \sum_i \Delta s(c_i,t) \leq (|\mathscr{N}|-1)t+1, \tag{11}$$

$$D(t) = \sum_i d(c_i,t) \leq |\mathscr{N}|^t, \tag{12}$$

where $|\mathscr{N}|$ denotes the size of the neighborhood (e.g. $|\mathscr{N}| = 3$ for ECA).

It is clear that in order to define Lyapunov exponents, we need to consider the number of ways in which defects can propagate to a certain cell instead of merely considering the number of defects occurring at a cell. As such, the defects are tracked in tangent space instead of configuration space. Now we can define the total Lyapunov exponent as[4]

$$\Lambda_1 = \lim_{t\to\infty} \frac{1}{t} \log\left(\frac{D(t)}{D(0)}\right). \tag{13}$$

In the maximally unstable case, every defect propagates to every cell in its neighborhood at the next time step. This implies that all Boolean derivatives in the Jacobian are then non-zero, which yields a defect pattern whose entries constitute the trinomial triangle. Since the sum of the elements of the nth row of this triangle equals 3^n, the total Lyapunov exponent for the maximally unstable cases equals $\log(3)$. Generalizing this result to CA with an arbitrary neighborhood size, we find that the total Lyapunov exponent is constrained to $\{-\infty\} \cup [0, \log(|\mathscr{N}|)]$.

The total Lyapunov exponent characterizes the global stability of the CA. However, we may also be interested in how the defects propagate to the different parts of the lattice. This additional spatial information is contained in the defect pattern $\boldsymbol{d}(t)$[1]. Applying the element-wise logarithm,

we obtain the finite-time Lyapunov profile[1]:

$$\mathbf{\Lambda}(i,T) = \frac{1}{T}\log(\boldsymbol{d}(i,T)). \tag{14}$$

$\mathbf{\Lambda}(T)$ constitutes a profile of N Lyapunov exponents, where N is the size of the lattice. In this sense, a CA on a finite lattice is considered as an N-dimensional discrete dynamical system, where every cell in the lattice corresponds to a single spatial dimension with a corresponding Lyapunov exponent. The elements of $\mathbf{\Lambda}(T)$ represent the averaged exponential growth rate of the number of defects at every cell due to the introduction of an initial defect at the center of the lattice.

Note that in the original definition of the Lyapunov spectrum of a dynamical system, an infinitesimally small perturbation is introduced in each of the N dimensions. The Lyapunov spectrum is then defined as the set of eigenvalues of the product of the system's corresponding Jacobian and its transpose[20]. The N different eigenvalues correspond to the different growth rates of the N possible (mutually orthogonal) perturbations one can introduce. When computing the Lyapunov exponents of a CA, the aforementioned product of the Jacobians is multiplied by a single seed vector consisting of all zeroes and a single non-zero entry at the center, which indicates that the perturbation happens in only a single dimension (i.e. the cell at the center of the lattice). This is justified since, in contrast to general dynamical systems, every dimension (i.e. every cell) is treated precisely the same by the CA's dynamics. This means that, for a large enough random initial configuration, the global features of the Lyapunov profile do not depend on which cell is initially perturbed. Additionally, perturbing only a single cell has the advantage of preserving the spatial information regarding the spreading of the defects to neighbouring cells. Nevertheless, computing the Lyapunov spectrum of a CA by diagonalizing the product of the Jacobians may be interesting and complementary to the approach outlined here, as it would essentially provide a statistical distribution of the Lyapunov exponents and allow us to extend results regarding the Lyapunov dimension to the framework of CA[12].

The equivalence of the different dimensions (i.e. cells) in phase space to one another also has the consequence that the global features of the Lyapunov profile are independent of the choice of the random initial configuration when the size of the grid is large enough.

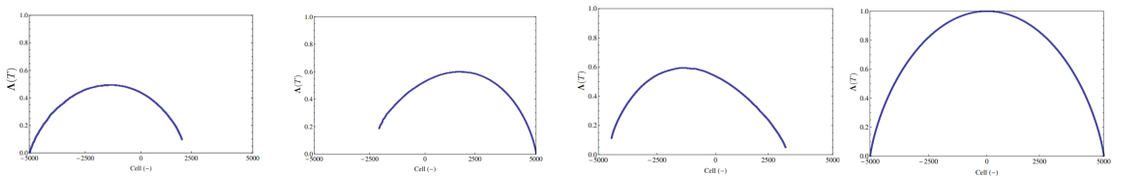

(a) (b) (c) (d)

FIG. 2: Normalized Lyapunov profiles of ECA rules 6 (a), 30 (b), 110 (c) and 150 (d). Reproduced with permission from Journal of Cellular Automata 13, (2015). Copyright 2015 Old City Publishing.

C. Two-state CA: examples

For ECA rule 150, all Boolean derivatives are 1, which indicates that every defect propagates to its three neighboring cells at the next time step. Because of this, the Lyapunov profile of rule 150 is maximal. The value of the profile near the center equals $\frac{1}{t}\log_2\binom{t}{0}^1$. This upper limit allows us the normalize the Lyapunov profiles of ECA. Figure 2 shows the normalized Lyapunov profiles of different ECA. For Class III rules 90 and 150, the difference pattern grows at a maximal rate of $|\mathcal{N}|-1$ cells per time step. This yields a Lyapunov profile that is non-zero across the entire lattice. This is not the case for all Class III rules. For example, rule 30 has a Lyapunov profile with a sharp transition to $-\infty$ near the left of the lattice (Fig. 2b). This indicates that the difference pattern is asymmetric and propagates at the maximal rate to the right but at a slower rate to the left.

Generally, the difference pattern of Class II rules is limited to a certain region. This yields a Lyapunov profile that equals $-\infty$ across most of the lattice, except for some cells where the difference pattern persists. However, there are certain exceptions such as Class II rules 6 (Fig. 2a) and 38, which are stable yet have non-trivial non-zero Lyapunov profiles. Such a discrepancy between the stability of a CA and its Lyapunov exponent is analogous to the Perron effect from dynamical systems theory[15]. Class IV rules such as rule 110 yield Lyapunov profiles that are similar to those of Class III, with a sharp transition to $-\infty$ usually on one side of the lattice (Fig. 2c).

Note that the above definition of the Lyapunov profile is immediately extendable to higher dimensional lattices. For instance, Figure 3 shows the Lyapunov profile corresponding to the two-dimensional equivalent of ECA rule 150.

Clearly, Eqs. (4) and (10) rely on Boolean arithmetic since there is only one type of defect (a $0 \to 1$

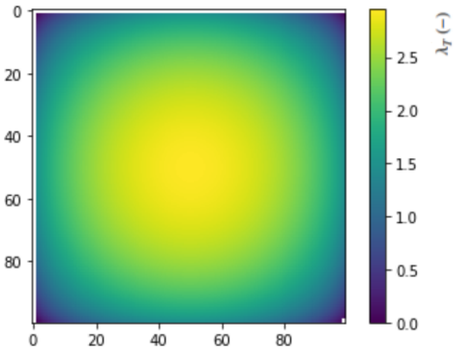

FIG. 3: Lyapunov profile of a two-dimensional version of rule 150.

defect). However, when we consider a CA with three or more states, there are multiple pairs of states between which a transition is possible. Generally there are $k(k-1)/2$ defects possible for a k-state CA. Furthermore we can also account for the directionality of defects. This means that, for example, a $1 \to 0$ defect is considered to be distinct from a $0 \to 1$ defect. This yields a total of $k(k-1)$ possible defects for a k-state CA. Consequently, Eqs. (4) and (10) are not applicable to CA with three or more states.

In the following section, we discuss how these equations can be extended to the multi-state case while additionally taking the directionality of defects into account.

D. Multi-state CA

Generalizing the definition of Lyapunov exponents for two-state CA to k-state CA, while also taking the directionality of the defects into account, will lead to $k(k-1)$ Lyapunov exponents. Each exponent quantifies the average exponential growth rate of one of the $k(k-1)$ types of defects. Our approach is illustrated using the three-state totalistic CA with rule number 420 according to Wolfram's numbering convention. This rule is chosen since it yields maximal Lyapunov profiles as its Boolean derivatives are all non-zero. The rule table of this CA is shown in Table I. In such a table, all possible values of the sum of the cells in the neighborhood of a cell c_i are listed, along with the corresponding update value of cell c_i.

The extension of the Lyapunov profiles to multi-state CA requires a change in how the entries of the Jacobian $\boldsymbol{J}(\boldsymbol{s}(t),t)$ are defined. Now, in addition to the Boolean partial derivatives of the transition function $\phi : S^{|\mathscr{N}|} \to S$, $\boldsymbol{J}(\boldsymbol{s}(t),t)$ in Eq. (2) contains also a symbolic label $\tau_{v\to w}$ to track

$\sum_{i=-1}^{\lvert\mathscr{N}\rvert} s(c_i,t)$	6	5	4	3	2	1	0
$s(c_0,t+1)$	0	1	2	0	1	2	0

TABLE I: Rule table for totalistic rule 420

the type of defect that occurs:

$$\big[\boldsymbol{J}(\boldsymbol{s}(t),t)\big]_{ij} = \begin{cases} \tau_{v\to w}, & \text{if } \phi\big(\tilde{s}(\mathscr{N}(c_i),t)\big) \neq \phi\big(\tilde{s}_{j,v\to w}(\mathscr{N}(c_i),t)\big)\,, \\ 0, & \text{if } \phi\big(\tilde{s}(\mathscr{N}(c_i),t)\big) = \phi\big(\tilde{s}_{j,v\to w}(\mathscr{N}(c_i),t)\big)\,. \end{cases} \tag{15}$$

Here, $\tilde{s}_{j,v\to w}(\mathscr{N}(c_i),t)$ is the tuple obtained by perturbing $s(c_j,t)$ from state v to state w in the tuple $\tilde{s}(\mathscr{N}(c_i),t)$. The state values of v and w depend on the type of defect arriving at cell c_i at time t.

We have the same update equation governing the time evolution of $\boldsymbol{d}(t)$:

$$\boldsymbol{d}(t+1) = \boldsymbol{J}(\boldsymbol{s}(t),t)\boldsymbol{d}(t)\,, \tag{16}$$

where regular matrix multiplication takes place. Given that $\tau_{v\to w}$ is a symbolic label, the elements of $\boldsymbol{d}(t)$ are polynomials in $\tau_{v\to w}$. We denote the polynomial at cell c_i at time step t as $\mathscr{P}_i^t(\tau_{v\to w})$. Each term in $\mathscr{P}_i^t(\tau_{v\to w})$ represents a defect path that arrives at cell i in t time steps. The exponent of $\tau_{v\to w}$ in such a term represents the number of times the defect $\tau_{v\to w}$ occurs in this defect path.

Figure 4 shows the space-time pattern generated by totalistic rule 420 starting from a random initial configuration of seven cells evolved over three time steps. The central cell of the initial configuration is perturbed from 0 to 2. The subsequent defect propagation yields defects at an increasing number of cells at each subsequent time step. There are three arrows going from the initial defect at $t = 0$ to the configuration at $t = 1$; all three Boolean derivatives are non-zero because:

$$\phi\big(\{1,0,\mathbf{0}\},t=0\big) \neq \phi\big(\{1,0,\mathbf{2}\},t=0\big) \tag{17}$$

$$\phi\big(\{0,\mathbf{0},0\},t=0\big) \neq \phi\big(\{0,\mathbf{2},0\},t=0\big) \tag{18}$$

$$\phi\big(\{\mathbf{0},0,0\},t=0\big) \neq \phi\big(\{\mathbf{2},0,0\},t=0\big). \tag{19}$$

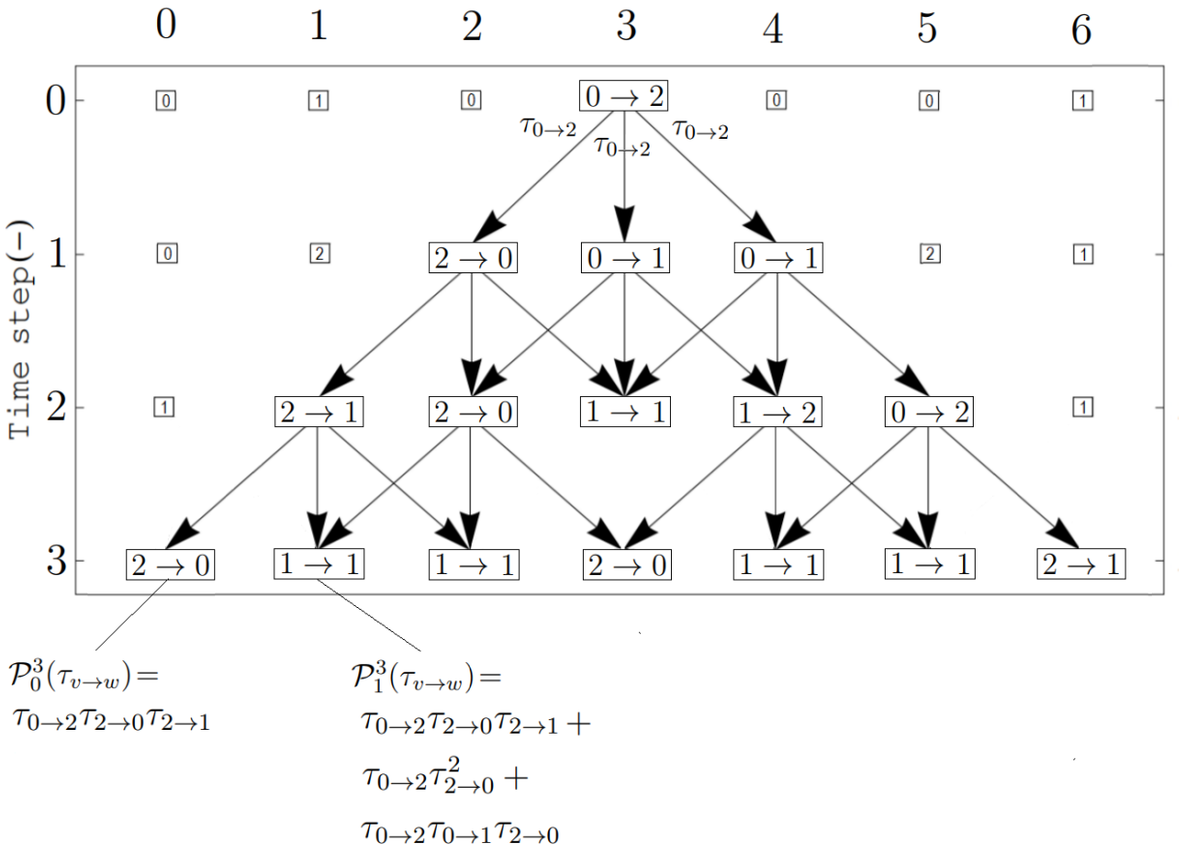

FIG. 4: Schematic representation of how an initial defect introduced at cell 3, t = 0 propagates throughout the lattice, for the case of totalistic three-state rule 420.

Recall that totalistic rule 420 was chosen precisely because its Boolean derivatives are always 1, yielding maximal defect spreading. This means that all defects at all cells will propagate to their three neighboring cells. The arrows in Figure 4 are labelled by the type of defect that is being propagated. For simplicity, only the first three defect arrows are labelled in Figure 4. In some instances, there are two or more defect arrows arriving at a cell, yet there is no defect present at this cell. For instance, this is the case at cell three at time step $t = 2$ in Figure 4 and occurs when two or three defects interact in such a way that they cancel each other out. Naturally, as there is no defect present at such a cell, there are no outgoing defect arrows. So missing outgoing defect arrows point to either a zero-valued Boolean derivative or multiple defects cancelling each other out.

Let us now provide a better understanding of the polynomials' structure. For instance, as shown in Figure 4, $\mathscr{P}_0^3(\tau_{v\to w})$ equals $\tau_{0\to2}\tau_{2\to0}\tau_{2\to1}$, which indicates that there is a single defect path

arriving at cell $c_i = 0$ at time step $t = 3$. Moreover, it consists of three different defects $\tau_{0\to2}$, $\tau_{2\to0}$ and $\tau_{2\to1}$. When moving towards the center of the lattice, where the defect was introduced, the number of defect paths arriving at a certain cell increases. Indeed,

$$\mathscr{P}_1^3(\tau_{v\to w}) = \tau_{0\to2}\tau_{2\to0}\tau_{2\to1} + \tau_{0\to2}\tau_{2\to0}^2 + \tau_{0\to2}\tau_{0\to1}\tau_{2\to0}.$$

Now there are three terms in this polynomial, indicating that three defect paths arrive at cell $c_i = 1$ at the third time step, the first consisting of a $0 \to 2$, $2 \to 0$ and $2 \to 1$ defect, the second of a $0 \to 2$ defect and two $2 \to 0$ defects, and the third of a $0 \to 2$, $0 \to 1$ and $2 \to 0$ defect. The sum of the exponents of each term in the polynomial equals the number of defects comprising the defect path, which will always equal the number of time steps. In the two-state case, the Jacobian contained ones and zeroes, yielding only the number of defect paths arriving at a given cell. Here, this number is given by the number of terms in a polynomial at a given cell.

For the sake of comprehensiveness, we introduce the notation $\sum(\mathscr{P}_i^t(\tau_{v\to w}), q \to r)$ to denote the sum of the exponents of every $\tau_{q\to r}$ variable in $\mathscr{P}_i^t(\tau_{v\to w})$. For example, for totalistic rule 420 we obtain for the $2 \to 0$ defect the following for cells $c_i = 0$ and $c_i = 1$

$$\sum\left(\mathscr{P}_0^3(\tau_{v\to w}), 2 \to 0\right) = 1 \tag{20}$$

$$\sum\left(\mathscr{P}_1^3(\tau_{v\to w}), 2 \to 0\right) = 1+2+1 = 4. \tag{21}$$

Note that this reduces to the familiar approach applied to two-state rules when considering the number of terms (i.e. the number of defect paths) that occur in each polynomial: the results above would be 1 and 3 respectively. Now we get additional information since we are not only interested in the number of defect paths, but also the kind of defects that the paths consists of, which is reflected by the size of each of the terms occurring in the sums in Eq. (20) and (21).

Finally, we may introduce the finite-time Lyapunov profile associated with defect $q \to r$ as follows:

$$\mathbf{\Lambda}_{q\to r}(i,T) = \frac{1}{T}\log\left(\sum\left(\mathscr{P}_i^T(\tau_{v\to w}), q \to r\right)\right). \tag{22}$$

Note that this approach is readily applicable to both deterministic and probabilistic CA.

In addition to considering the full Lyapunov profile that corresponds to a specific defect pattern,

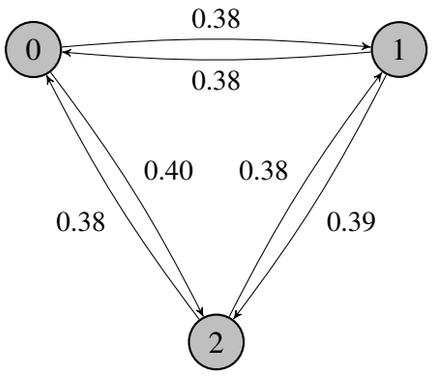

FIG. 5: Average Lyapunov exponents for totalistic rule 420.

we may consider the average Lyapunov exponent (ALE) by averaging the $k(k-1)$ total Lyapunov exponents across many initial configurations. In this way, we obtain an overview of the average propagation of defects. The ALEs for rule 420 are shown in Figure 5. Due to the chaotic nature of rule 420, the six different ALEs have similar values.

It should also be noted that while the Lyapunov exponents provide a comprehensive overview of how different kinds of defects propagate, they fail to capture whether the defect cone grows regularly or irregularly. One way to capture this is by plotting the size of the defect pattern (i.e. the sum of its entries) at time step t versus the size of the defect pattern at $t+1$. Figure 6 shows the space-time pattern generated by rule 421 together with the corresponding defect pattern and defect pattern growth plot. Note that totalistic rule 421 was chosen instead of totalistic rule 420 as the latter would not be particularly enlightening due to its unique difference pattern, which is a consequence of its additive property.

In the following section, we illustrate this newly proposed approach for some exemplary totalistic three-state rules, to demonstrate the utility of the additional insights our approach can provide.

III. BEHAVIORAL ANALYSIS OF MULTI-STATE CA

A. Experimental setup

For each of the totalistic three-state rules considered in this section, the propagation of defects emerging from a single defect was tracked for 75 time steps in a one-dimensional system consisting of 150 cells. Every simulation starts from a random initial configuration with a single initial

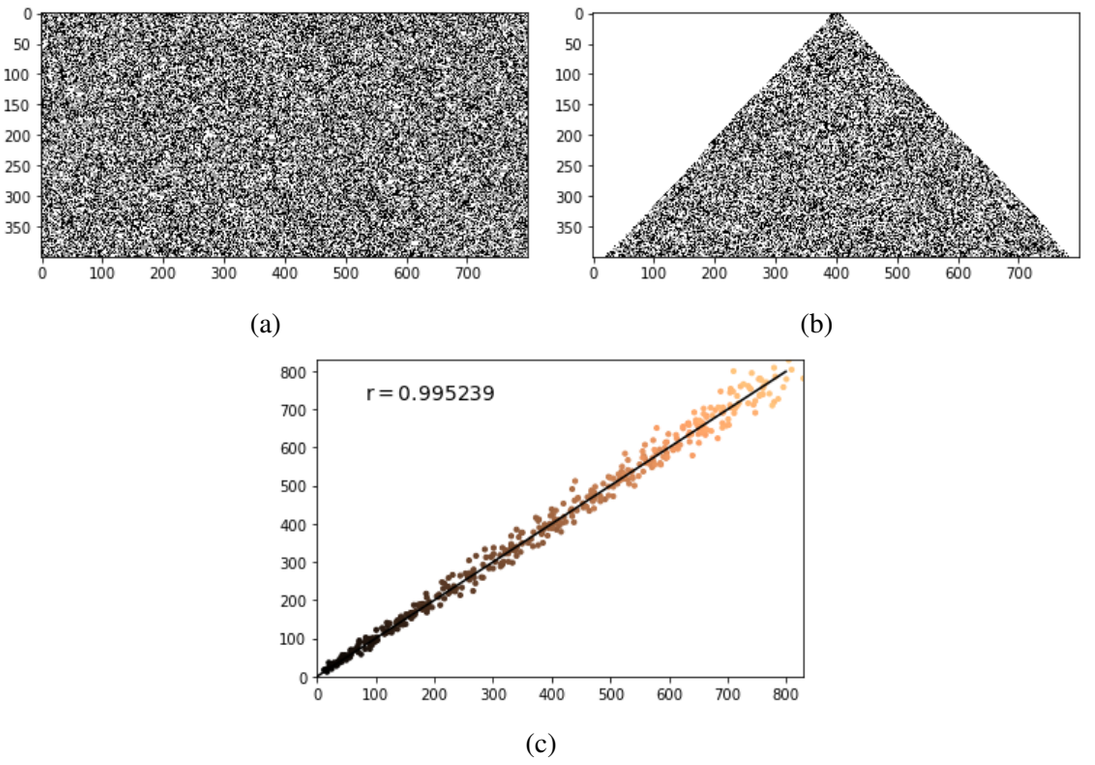

FIG. 6: The space-time pattern (a) generated by rule 421 together with the corresponding defect pattern (b) and defect pattern growth plot (c).

defect at the center of the lattice. Note that the Lyapunov profiles generally depend on the initial configuration from which they are evolved, however for a large enough lattice size, this dependence becomes negligible.

For the sake of clarity, the discrete points in the Lyapunov profiles are connected by lines. A single totalistic three-state rule is chosen from each of Wolfram's classes[30], and its original space-time pattern, defect pattern and Lyapunov profiles are computed. Rules with short transients are chosen, so that the Lyapunov profiles reflect the steady-state behavior of their corresponding rule. When averaging the profiles over the $k(k-1)$ posssible defects, the results regarding defect spreading in the different Wolfram classes are similar to those obtained in the ECA case described in Section II B. However, distinguishing between the different defect types and introducing a Lyapunov profile for each of these types gives us additional interesting insights.

B. Phenomenology

1. Class I

The rules in Class I demonstrate trivial behavior. Examples include rules 135, 252 and 279. After a transient, the difference pattern vanishes which yields a Lyapunov profile that is zero everywhere. Any perturbation to the initial configuration dies out and the system converges to the same equilibrium configuration.

2. Class II

After a short transient, Class II rules yield a periodic difference pattern that generally depends on the initial configuration. As it is periodic, the difference pattern is non-expanding, which means the initial perturbation can only affect cells within a certain finite region. In this region the Lyapunov profile is non-zero. The types of defects that tend to occur in the periodic region of the difference pattern is reflected in differences in magnitude between the Lyapunov profiles corresponding to different defect types. This is illustrated in Figure 7b for rule 126, where the $1 \rightarrow 0$ defects make up an important part of the periodic region of the defect pattern, as this is reflected in the corresponding Lyapunov profile in Figure 7c. Additionally, it is clear that the Lyapunov profile is non-zero only in those regions of the lattice where the periodic part of the defect pattern persists.

3. Class III

The difference patterns associated with Class III rules are expanding. The difference pattern growth rate often approaches the upper bound of $|\mathcal{N}|-1$ cells per time step. The typical Lyapunov profiles associated with such a difference pattern are shown for rule 420 in Figure 8. As Class III CA are chaotic, the profiles are non-zero across the entire lattice and are largely overlapping since the different defect types are randomly and uniformly distributed over the difference pattern. The profiles reach their maximal value near the cell where the initial perturbation was introduced, since the number of paths reaching this cell is maximal.

The Lyapunov profiles have a typical shape which is independent of the initial configuration, which is analogous to their typical white noise power spectrum[18]

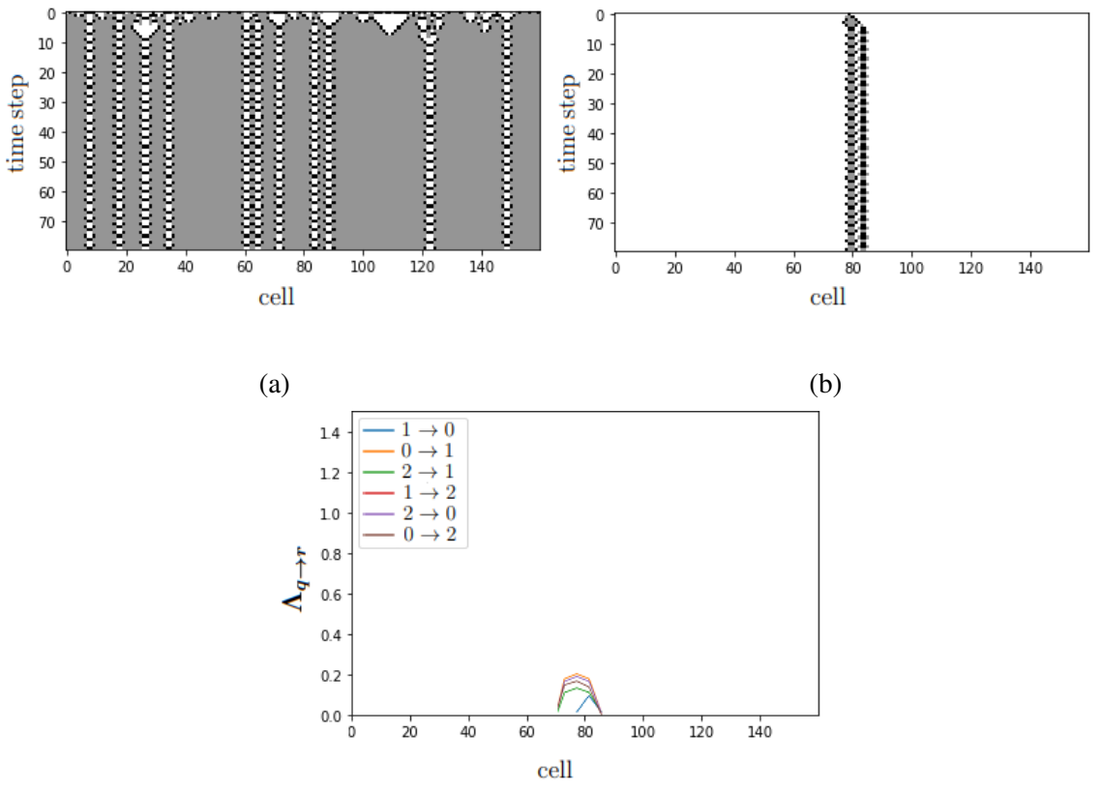

FIG. 7: The space-time pattern (a), defect pattern (b) and Lyapunov profiles for the six defect types (c) generated by Class II rule 126.

4. Class IV

Often, Class IV CA are considered to lie in the transition region between Class II and Class III CA[14,29,31]. This is reflected in the fact that their Lyapunov profiles have characteristics of those associated with both classes. The difference pattern is expanding, yet often at a highly variable rate that is significantly below the the upper bound of $|\mathcal{N}| - 1$ cells per time step. This yields Lyapunov profiles that are non-zero only in certain parts of the lattice while, similarly to Class II Lyapunov profiles, a sharp transition to zero may occur. This is illustrated for rule 231 in Figure 9.

Unlike Class III profiles which have a single maximum near the cell where the perturbation was introduced, Class IV CA may have multiple local extrema. This is illustrated for Class IV rule 114 in Figure 10. A local minimum in the Lyapunov profiles indicates the splitting of the difference pattern into two clusters, which can be seen in Figure 10c. During the time evolution of a Class IV

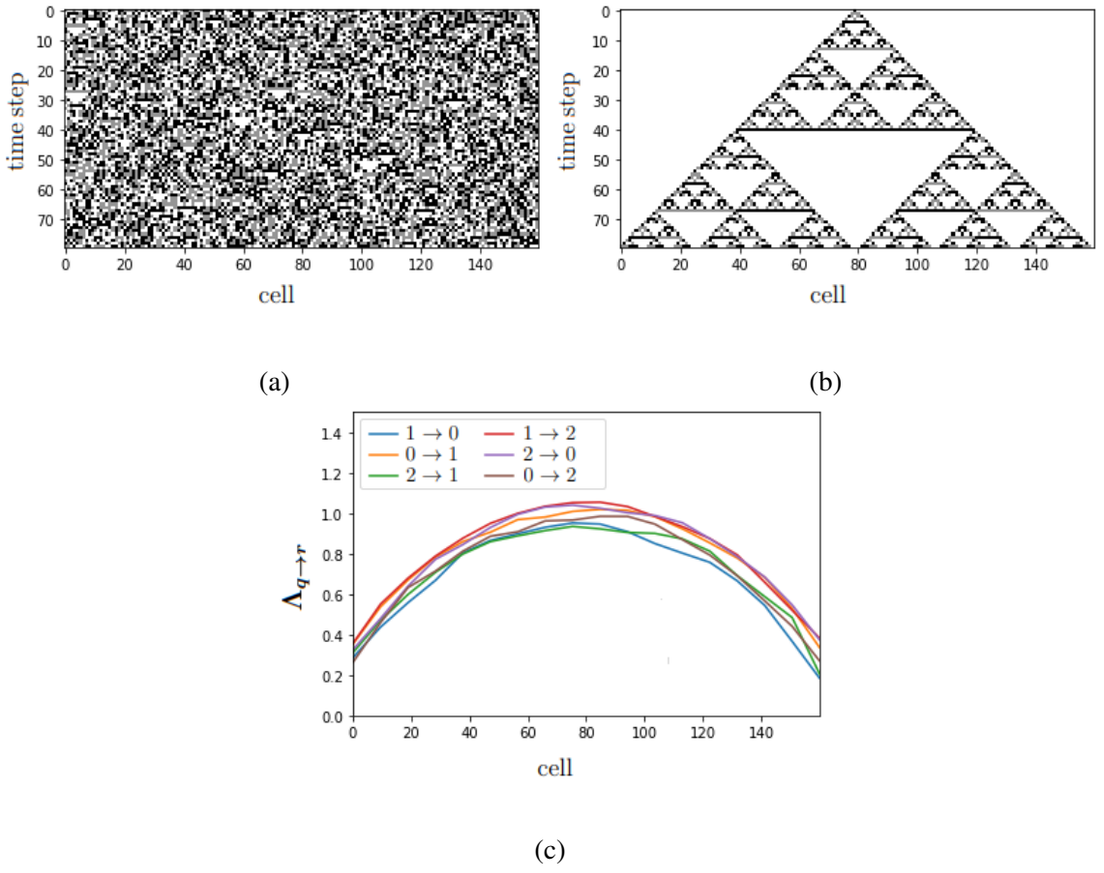

FIG. 8: The space-time pattern (a), defect pattern (b) and Lyapunov profiles for the six defect types (c) generated by Class III rule 420.

rule, any number of such clusters can emerge and often they collide again at a later time. This yields an ever changing number of local extrema in the Lyapunov profile as time progresses, so the finite time Lyapunov profiles of Class IV rules strongly depend on the considered number of time steps. This is to be expected, as Class IV is often regarded as CA with an infinite transient (i.e. no steady-state behavior)[29].

Additionally, the Lyapunov profile of a Class IV CA often depends highly on the type of defect that is considered. This is illustrated for Class IV rule 63 in Figure 11, where it is clear that the Lyapunov profile associated with the $2 \to 0$ defect dominates. This indicates that, for large simulation times, any defect path will consist nearly entirely of $2 \to 0$ defects.

The distinct properties of Class IV Lyapunov profiles allows us to distinguish Class IV CA from Class III CA, which has otherwise been proven to be exceptionally difficult[29,31].

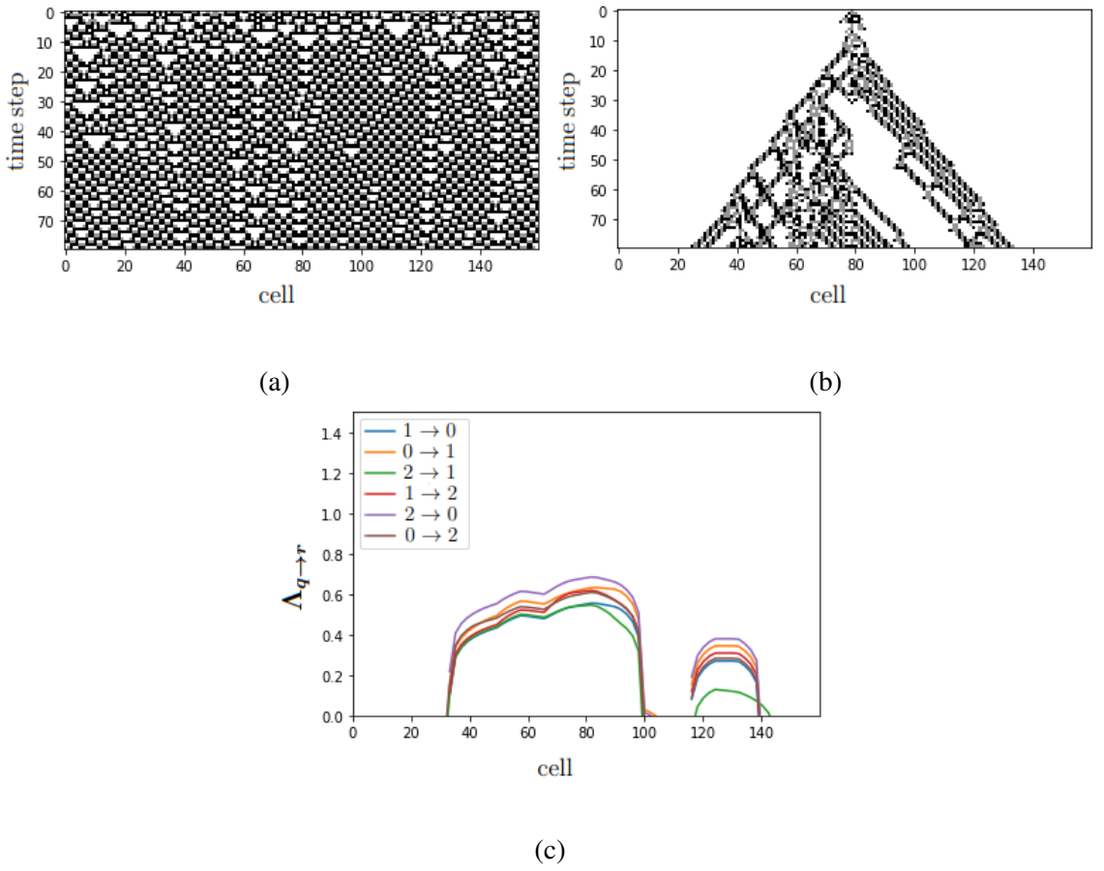

FIG. 9: The space-time pattern (a), defect pattern (b) and Lyapunov profiles for the six defect types (c) generated by Class IV rule 231.

C. Average Lyapunov exponents

The $k(k-1)$ ALEs summarize the average propagation of defects by providing the average value of the total Lyapunov exponents when computed for many different initial configurations. This information can be conveniently represented in a state transition graph where the k nodes represent the CA state space and the arrows between them indicate the ALE of the corresponding defect.

Figure 12b shows the state transition graph for Class III totalistic 4-state rule 120 and the ALEs retrieved by considering 100 different random initial configurations. All ALEs have a value close to 0.5, so this state transition diagram indicates that any kind of initial defect propagates throughout the lattice by causing all possible defects with a similar relative frequency.

Figure 12b shows the state transition graph for Class II totalistic 4-state rule 70, where again the ALEs were computed by averaging over 100 different initial configurations. In this case, there is

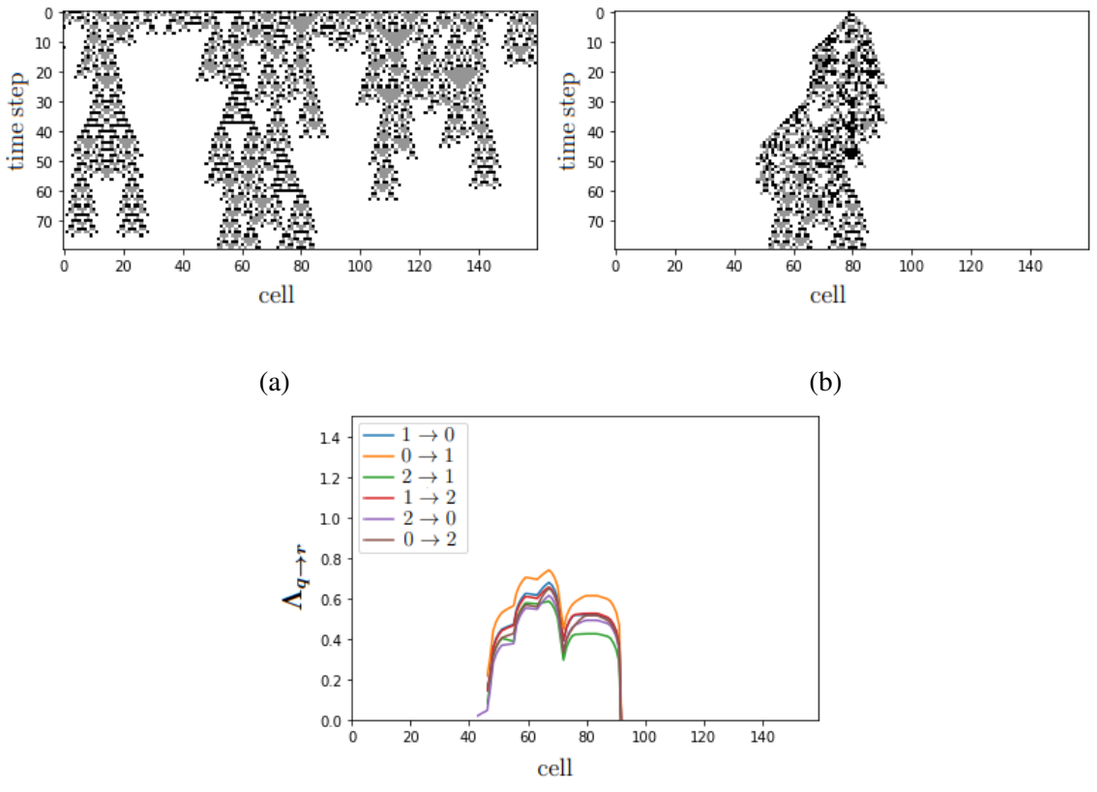

FIG. 10: The space-time pattern (a), defect pattern (b) and Lyapunov profiles for the six defect types (c) generated by Class IV rule 114.

a clear variation in the values of the different ALEs. Some defects yield vanishing ALEs in both directions (e.g. $1 \to 3$ and $3 \to 1$), while others yield a vanishing ALE only in a single direction (e.g. $2 \to 3$).

D. Growth of the difference pattern

By plotting the size of the defect pattern at time step t versus the size of the defect pattern at time step $t+1$, we obtain additional useful information about whether or not the defect cone grows regularly or irregularly.

When the difference pattern grows at a relatively regular rate, the points in the scatter plot tend to hover closely around the diagonal $y = x$, which is reflected by a high Pearson correlation coefficient. Conversely, irregular growth will ensure that points are scattered farther from diagonal,

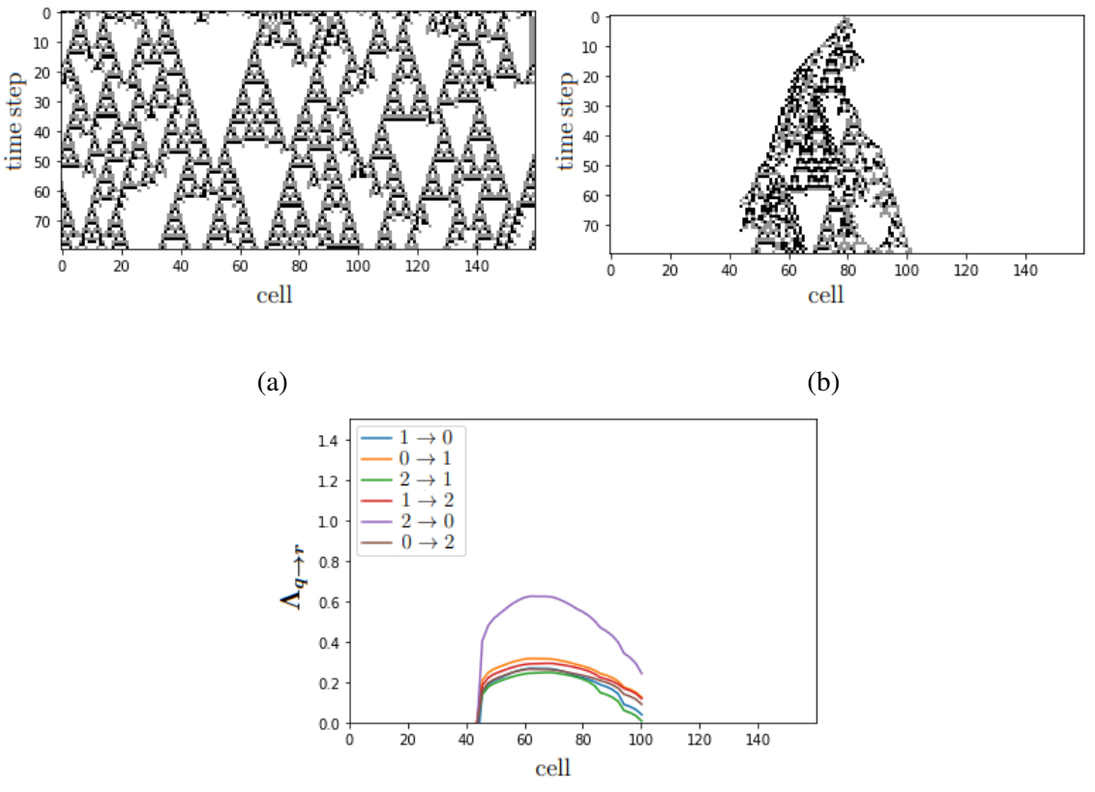

FIG. 11: The space-time pattern (a), defect pattern (b) and Lyapunov profiles for the six defect types (c) generated by Class IV rule 63.

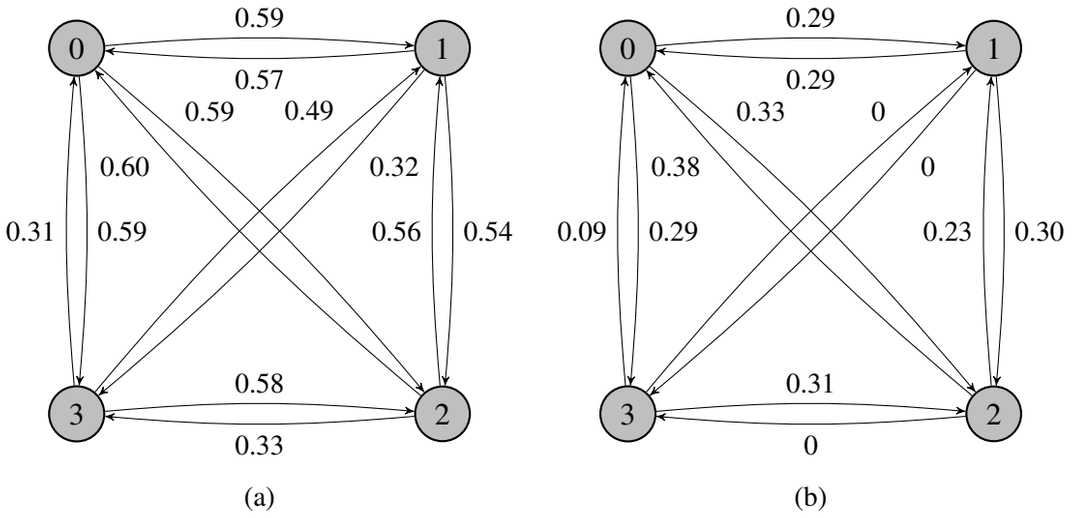

FIG. 12: Average Lyapunov exponents for totalistic 4-state rules 120 (a) and 70 (b) represented using a state transition graph.

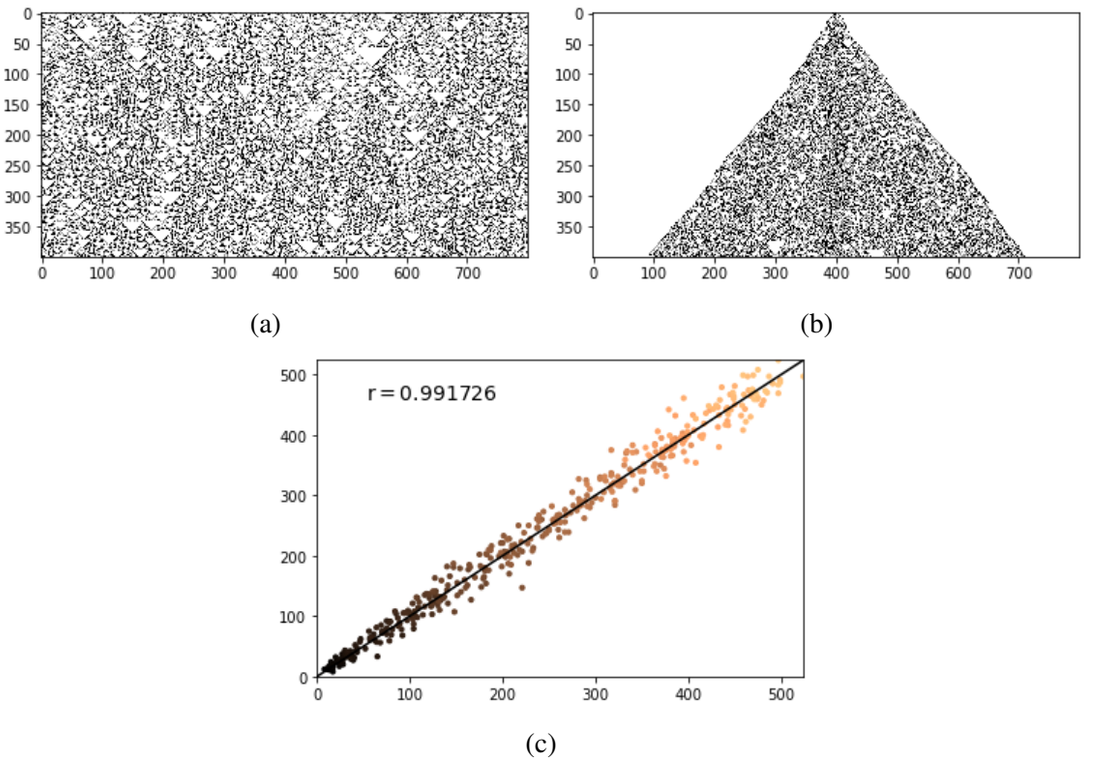

(a) (b) (c)

FIG. 13: The space-time pattern (a) generated by three-state totalistic rule 300 together with the corresponding defect pattern (b) and defect pattern growth plot (c).

yielding a lower Pearson correlation coefficient.

Below, we illustrate the usefulness of this concept for some totalistic three-state rules. Figure 13 shows the space-time pattern, defect pattern and corresponding defect pattern scatter plot for 400 time steps generated by Class III rule 300. The points in the scatter plot are colored according to the time step to which they correspond: darker colours indicate earlier time steps. The defect pattern grows regularly, leading to points clustered closely around the diagonal and a Pearson correlation coefficient very close to 1.

On the other hand, Figure 14 shows Class III rule 136, which is similarly chaotic, but has a defect pattern that grows more irregularly. This is reflected in a scatter plot with a lower Pearson correlation coefficient. For some rules, the defect pattern fluctuates between extended periods of growth and periods of contraction. This is reflected by the emergence of two clusters in the scatter plot, one at each side of the diagonal, as shown in Figure 15 for rule 69.

Finally, there are also additive CA, which lead to unique defect patterns such as the one shown for

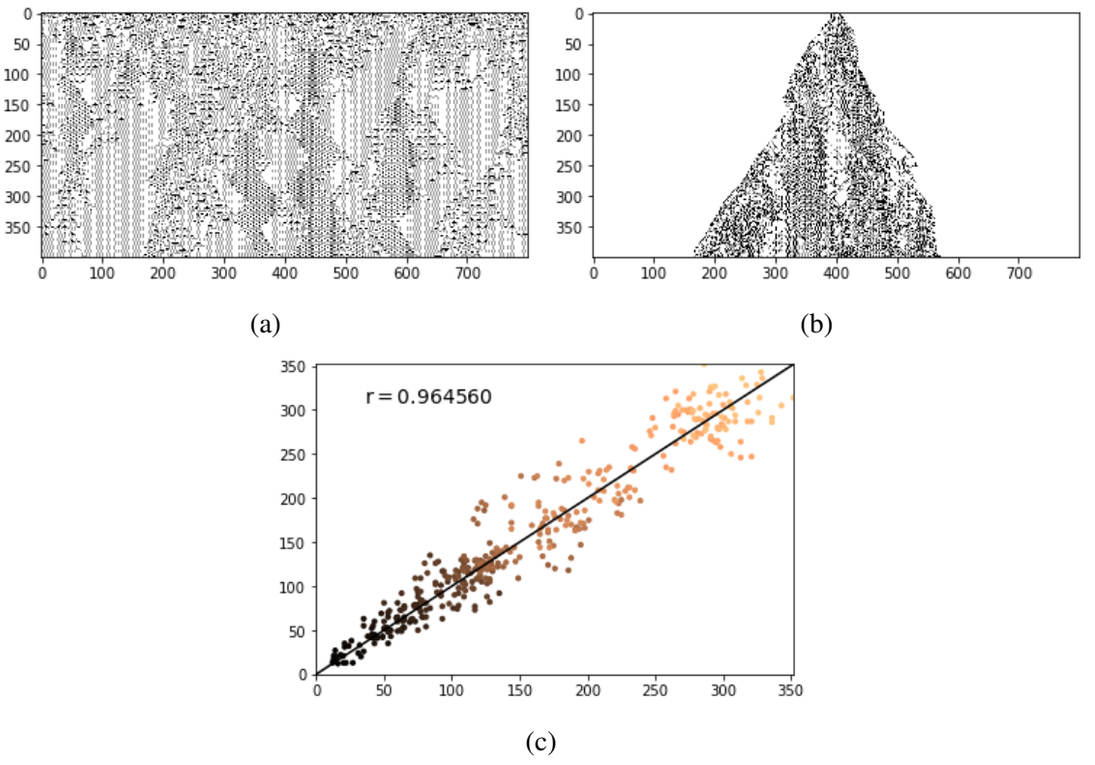

FIG. 14: The space-time pattern (a) generated by three-state totalistic rule 136 together with the corresponding defect pattern (b) and defect pattern growth plot (c).

Class III rule 170 in Figure 16b. The appearance of white triangular clearings in the defect pattern yields a scatter plot with a low Pearson correlation coefficient but without any particular clustering.

IV. BEHAVIORAL ANALYSIS OF A CA-BASED FOREST FIRE MODEL

Many CA-based models require more than two states. Examples include disease spread models[21], excitable media models[16,22], and forest fire models[17]. This section shows how the multi-state Lyapunov exponents and the related concepts outlined in the previous sections can be used to provide a comprehensive overview of the stability and sensitivity of such CA-based models. In particular, we consider a deterministic two-dimensional three-state forest fire CA model.

Figure 17a illustrates the transition functions of the model schematically. Each cell either contains a non-burning tree (T), a burning tree (B) or is empty (E). A cell containing a tree will ignite at ind $t+1$ if any of its neighbors are burning at time step t. A cell that is burning at time step t will be removed at time step $t+1$, which means we assume that every tree burns for precisely one time

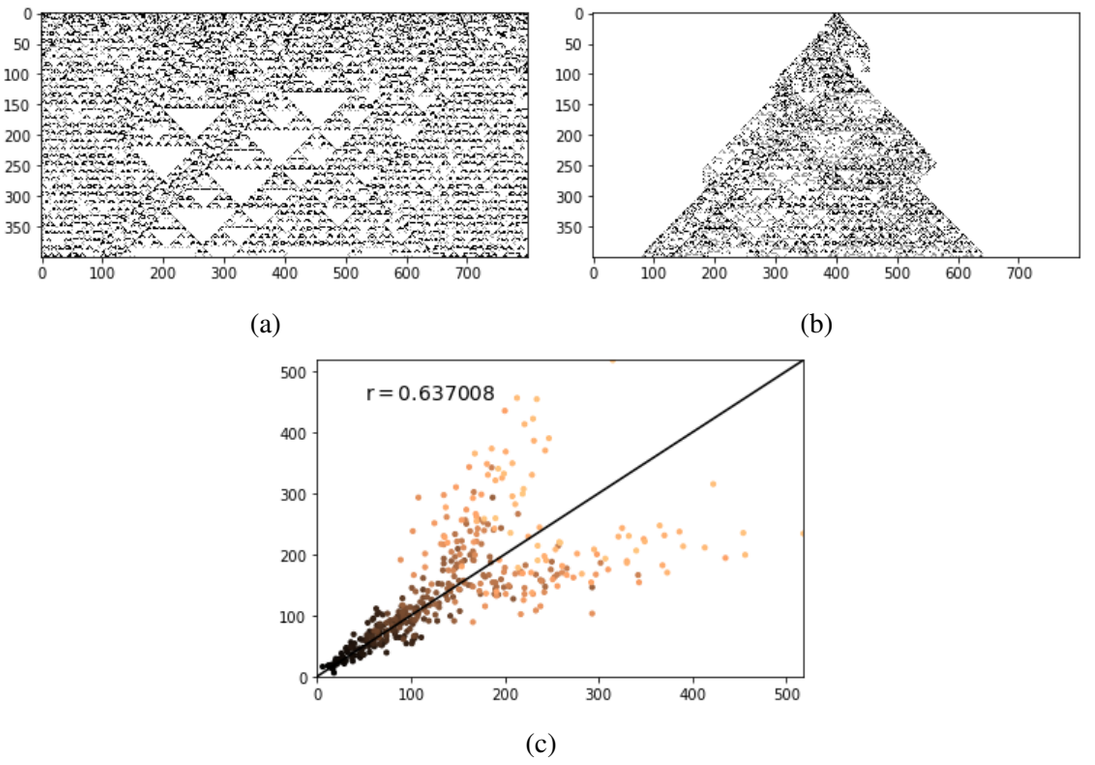

FIG. 15: The space-time pattern (a) generated by three-state totalistic rule 69 together with the corresponding defect pattern (b) and defect pattern growth plot (c).

step. An empty cell and a cell with a tree that does not have any burning neighbors will remain unchanged. Note that this CA belongs to Class IV in Wolfram's classification.

This model can be extended to make it more realistic by using a probabilistic update rule, shown schematically in Figure 17b. The probabilistic extension involves three changes to the deterministic model. Firstly, a tree without any burning neighbors can still ignite at the next time step with probability p_f. This takes into account the possibility that trees can catch fire due to overheating, lightning or human actions. Secondly, a burning tree will be removed at the next time step with probability p_b, which signifies that not all trees have the same burning time and thus accounts for individual variability between trees. Lastly, trees grow from an empty cell at the next time step with a probability p_g.

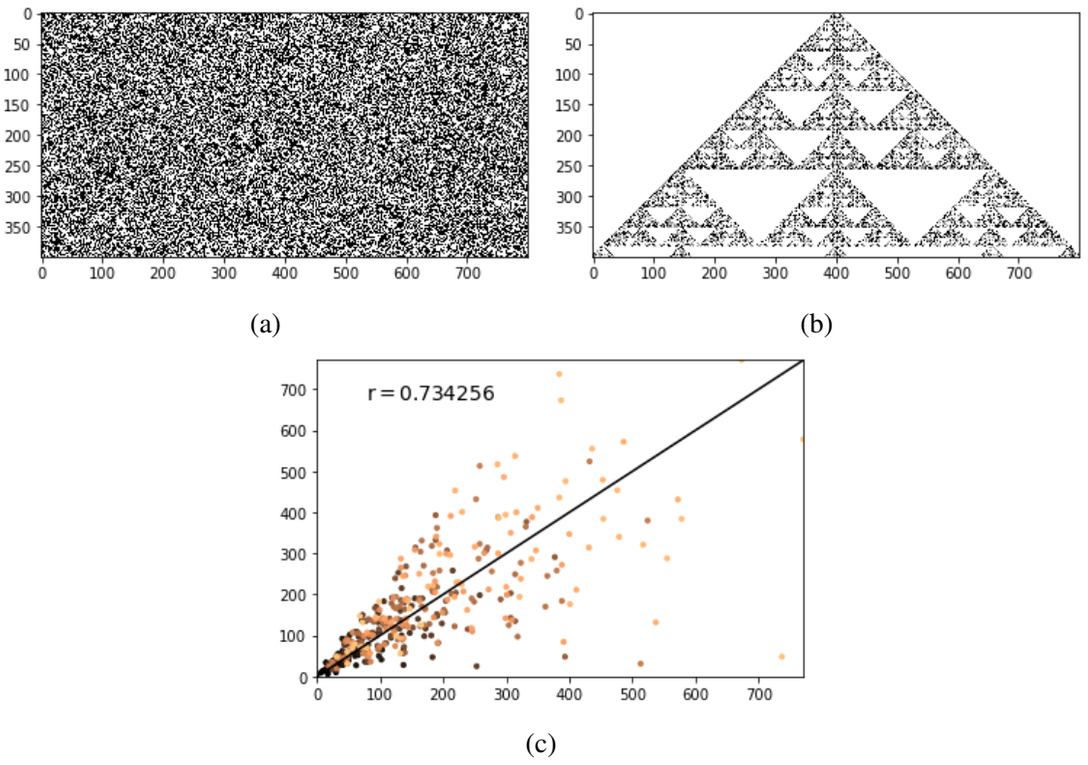

FIG. 16: The space-time pattern (a) generated by three-state totalistic rule 170 together with the corresponding defect pattern (b) and defect pattern growth plot (c).

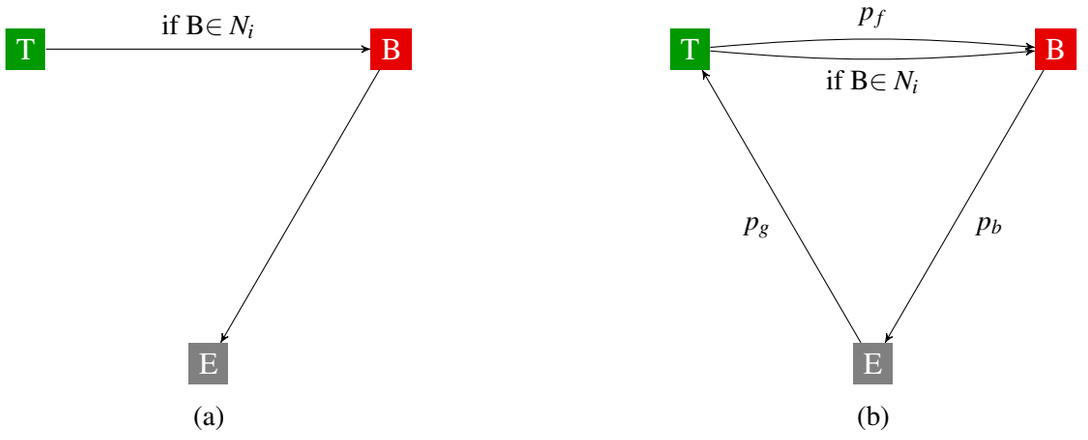

FIG. 17: Visual representation of the update rule for the deterministic (a) and probabilistic (b) forest fire model. The notation B$\in N_i$ is used to indicate that one of the neighbors of the cell is burning.

When simulating the forest fire spread, the density of trees in the initial configuration is inferred from p_d (i.e. the probability that a single cell is occupied by a tree is p_d). This parameter has a

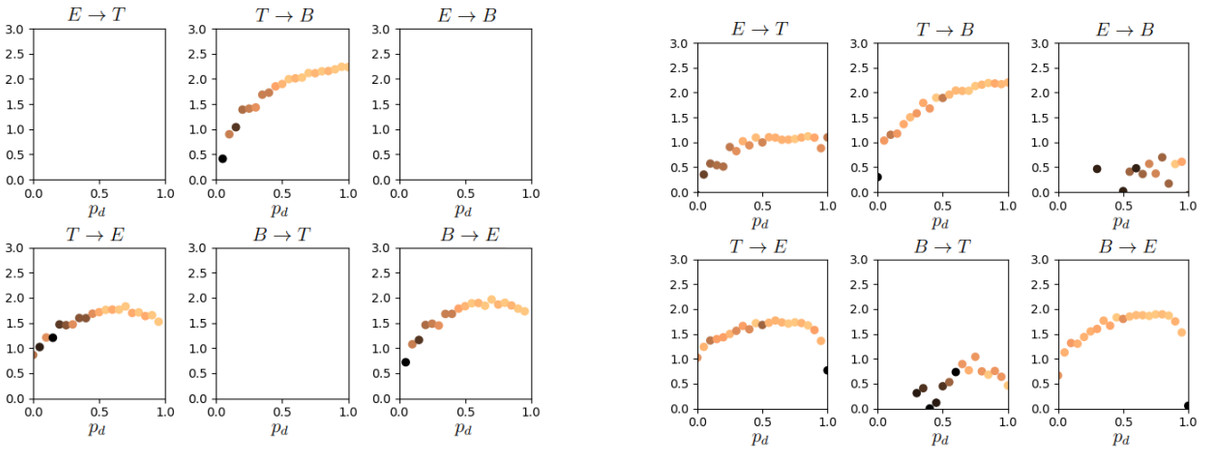

(a) (b)

FIG. 18: Average Lyapunov exponents as a function of p_d for the deterministic (a) and probabilistic (b) forest fire model. The points in the plot are colored according to the fraction of non-zero Lyapunov exponents: darker colours indicate that only a few Lyapunov exponents are non-zero

significant influence on the ability of the fire to spread and consequently on the sensitivity of the model to defects. As such, it is useful to look at the relationship between the Lyapunov exponents and p_d, which is shown in Figure 18. For every value of p_d, the ALEs are computed by averaging over 30 replicate simulations. For the probabilistic model, the values $p_f = 0.0005$, $p_g = 0.01$ and $p_b = 0.7$ were used. Each ALE value is coloured according to the number of non-zero Lyapunov exponents across the ensemble of 30 Lyapunov exponents. In the deterministic case, only those defects that are physically possible in the model are non-zero ($T \to E$, $T \to B$ and $B \to E$), i.e an empty cell cannot burn at any subsequent time step and an empty or burning cell cannot contain a tree at any subsequent time step. The ALE associated with the $T \to B$ defect increases monotonously with p_d. The ALEs associated with the $T \to E$ and $B \to E$ defects have a maximum value near $p_d \approx 0.7$. This indicates that the initial tree density can neither be too high nor too low in order to achieve the most efficient spreading of defects with an empty final state.

The results regarding $T \to E$, $T \to B$ and $B \to E$ defects are similar for the probabilistic extension of the model. However, now the $E \to T$, $B \to T$ and $E \to B$ defects are physically possible in the model as well. The $E \to T$ defect, which is now possible due to trees growing from an empty cell, is present and relatively independent of the initial tree density. The ALEs associated with $B \to T$ and $E \to B$ defects are also present yet relatively low, due to the fact that these states are further

apart in the model's state space (i.e. a burning cell first needs to become empty before it can grow a tree and an empty cell first needs to grow a tree before it may start to burn). Furthermore, there appears to be a cut-off value near $p_d \approx 0.5$, below which these defects are unable to spread.

Generally, our results indicate that the forest fire model will behave more chaotically when the initial tree density is higher. This is to be expected, as a higher initial tree density yields a model whose parts (i.e. cells) interact more strongly with one another.

V. CONCLUSIONS

In this paper, we have shown how the existing method of computing Lyapunov exponents of one-dimensional binary CA may be generalized to arbitrary deterministic or probabilistic N-dimensional k-state CA. In addition to generalizing the existing framework, our approach has the advantage that is distinguishes between the directionality of the defects. Furthermore, we introduced the ALE and the correlation coefficient associated with the difference pattern growth as concepts quantifying the sensitivity of the CA to initial perturbations. We applied our proposed approach to several three-state and four-state rules as well as a CA-based forest fire model. Depending on the specific CA, the Lyapunov profile, ALE and/or the correlation coefficient may be used to provide a comprehensive overview of the stability of the CA dynamics.

CA that are classified as Class IV in Wolfram's classification are generally the most interesting from both a theoretical and applied perspective. The Lyapunov profiles of these rules are particularly interesting as they or often dominated by a single type of defect, which indicates that Class IV CA may respond to a perturbation in a specific way. Additionally, the Lyapunov profiles of Class IV rules usually exhibit multiple local minima, indicating that the lattice is subdivided in multiple stable and unstable regions. Both of these particular features of Class IV Lyapunov profiles may be used to distinguish Class IV rules from Class III rules. This is a task that has confounded, and still confounds, many different classification techniques, while representing a key achievement in the characterization of CA.

ACKNOWLEDGMENTS

We acknowledge the support from the Special Research Fund of Ghent University, Belgium (Grant N01Z02016). The computational resources (Stevin Supercomputer Infrastructure) and services used in this work were provided by the VSC (Flemish Supercomputer Center), funded by Ghent University, FWO and the Flemish Government - department EWI.

AUTHOR DECLARATIONS

Conflict of Interest

The authors have no conflict of interest to disclose.

Author Contributions

M. Vispoel: Conceptualization (equal), Formal Analysis (equal), Data Curation (lead), Investigation (equal), Methodology (equal), Software (lead), Validation (equal), Visualization (lead), Writing - Original Draft Preparation (equal), Writing - Review & Editing (equal). **A. J. Daly**: Conceptualization (equal), Formal Analysis (equal), Investigation (equal), Methodology (equal), Project Administration (equal), Supervision (equal), Validation (equal), Writing - Original Draft Preparation (equal), Writing - Review & Editing (equal). **J. M. Baetens**: Conceptualization (equal), Formal Analysis (equal), Funding Acquisition (lead), Investigation (equal), Methodology (equal), Project Administration (equal), Resources (lead), Supervision (equal), Validation (equal), Writing – Original Draft Preparation (equal), Writing - Review & Editing (equal)

DATA AVAILABILITY

Data sharing is not applicable to this article as no new data were created or analyzed in this study.

REFERENCES

REFERENCES

[1]J. M. Baetens and J. Gravner. Introducing Lyapunov profiles of cellular automata. *Journal of Cellular Automata*, 13, 2015.

[2]F. Bagnoli and R. Rechtman. Synchronization and maximum lyapunov exponents of cellular automata. *Physical Review E*, 59:R1307–R1310, 1999.

[3]F. Bagnoli and R. Rechtman. Thermodynamic entropy and chaos in a discrete hydrodynamical system. *Physical Review E*, 79:041115, 2009.

[4]F. Bagnoli, R. Rechtman, and S. Ruffo. Damage spreading and Lyapunov exponents in cellular automata. *Physics Letters A*, 172:34 – 38, 1992.

[5]F. Bagnoli, R. Rechtman, and E. S. Yacoubi. Control of cellular automata. *Physical Review Letters E*, 86:066201, 2012.

[6]K. Bhattacharjee, N. Naskar, S. Roy, and S. Das. A survey of cellular automata: Types, dynamics, non-uniformity and applications. *Natural Computing*, 19:38–40, 2020.

[7]J. M. Comer, J. C. Cerda, D. D. Martinez, and D. H. K. Hoe. Random number generators using cellular automata implemented on FPGAs. In *Proceedings of the 2012 44th Southeastern Symposium on System Theory (SSST)*, pages 67–72, 2012.

[8]M. Courbage and B. Kaminski. Space-time directional Lyapunov exponents for cellular automata. *Journal of Statistical Physics*, 124, 2006.

[9]J.-C. Dubacq, B. Durand, and E. Formenti. Kolmogorov complexity and cellular automata classification. *Theoretical Computer Science*, 259:271–285, 2001.

[10]J. P. Eckmann and D. Ruelle. Ergodic theory of chaos and strange attractors. *Reviews of Modern Physics*, 57:617–656, 1985.

[11]Robert Fisch, Janko Gravner, and David Griffeath. Threshold-range scaling of excitable cellular automata. *Statistics and Computing*, 1:23–39, 1991.

[12]P. Frederickson, J.L. Kaplan, E.D. Yorke, and J.A. Yorke. The lyapunov dimension of strange attractors. *Journal of Differential Equations*, (2):185–207, 1983.

[13]A. Ilachinski. *Cellular Automata: A Discrete Universe*. World Scientific, 2001.

[14]C.G. Langton. Computation at the edge of chaos: Phase transitions and emergent computation. *Physica D: Nonlinear Phenomena*, 42:12–37, 1990.

[15]G.A. Leonov and N.V. Kuznetsov. Time-varying linearization and the perron effects. *International Journal of Bifurcation and Chaos*, 17:1079–1107, 2007.

[16]M. Markus and B. Hess. Isotropic cellular automaton for modelling excitable media. *Nature*, 347:56–58, 1990.

[17]K. Mutthulakshmi, M.R. En Wee, Y.C. Kester Wong, J.W. Lai, J.M. Koh, U. Rajendra Acharya, and K.H. Cheong. Simulating forest fire spread and fire-fighting using cellular automata. *Chinese Journal of Physics*, 65:642–650, 2020.

[18]S. Ninagawa. Power spectral analysis of elementary cellular automata. *Complex Systems*, 17:399–411, 2008.

[19]G. Oliveira, P. Oliveira, and N. Omar. Guidelines for dynamics-based parameterization of one-dimensional cellular automata rule spaces. *Complexity*, 6:63–71, 2000.

[20]V.I. Oseledets. A multiplicative ergodic theorem. characteristic lyapunov, exponents of dynamical systems. *Transactions of the Moscow Mathematical Society*, 19:179–210, 1968.

[21]B. Pfeifer, K. G. Kugler, M. M. Tejada, C. Baumgartner, M. Seger, M. Osl, M. Netzer, M. Handler, A. Dander, M. Wurz, A. Graber, and B. Tilg. A cellular automaton framework for infectious disease spread simulation. *The Open Medical Informatics Journal*, 2:70–81, 2008.

[22]L. Reyes and D. Laroze. Cellular automata for excitable media on a complex network: The effect of network disorder in the collective dynamics. *Physica A: Statistical Mechanics and its Applications*, 588:126552, 2021.

[23]C.R. Shalizi, R. Haslinger, J. Rouquier, K.L. Klinkner, and C. Moore. Automatic filters for the detection of coherent structure in spatiotemporal systems. *Physical Review E*, 73:036104, Mar 2006.

[24]M. A. Shereshevsky. Lyapunov exponents for one-dimensional cellular automata. *Journal of Nonlinear Science*, 2, 1992.

[25]S. Strogatz. *Nonlinear Dynamics and Chaos: With Applications to Physics, Biology, Chemistry and Engineering*. Westview Press, Boulder, United States, 2000.

[26]P. Tisseur. Cellular automata and Lyapunov exponents. *Nonlinearity*, 13:1547–1560, 2000.

[27]J. Vallejo and M. Sanjuán. *Predictability of Chaotic Dynamics: A Finite-time Lyapunov Exponents Approach*. 2019.

[28]G. Vichniac. Boolean derivatives on cellular automata. *Physica D: Nonlinear Phenomena*, 45:63–74, 1990.

[29]M. Vispoel, A. J. Daly, and J. M. Baetens. Progress, gaps and obstacles in the classification of cellular automata. *Physica D: Nonlinear Phenomena*, 432:133074, 2022.

[30]S. Wolfram. Universality and Complexity in Cellular Automata. *Physica D: Nonlinear Phenomena*, 1984.

[31]A. Wuensche. Classifying cellular automata automatically: Finding gliders, filtering, and relating space-time patterns, attractor basins, and the z parameter. *Complexity*, page 47–66, 1999.

AIP Publishing

Chaos
An Interdisciplinary Journal
of Nonlinear Science

PLEASE CITE THIS ARTICLE AS DOI: 10.1063/5.0139849

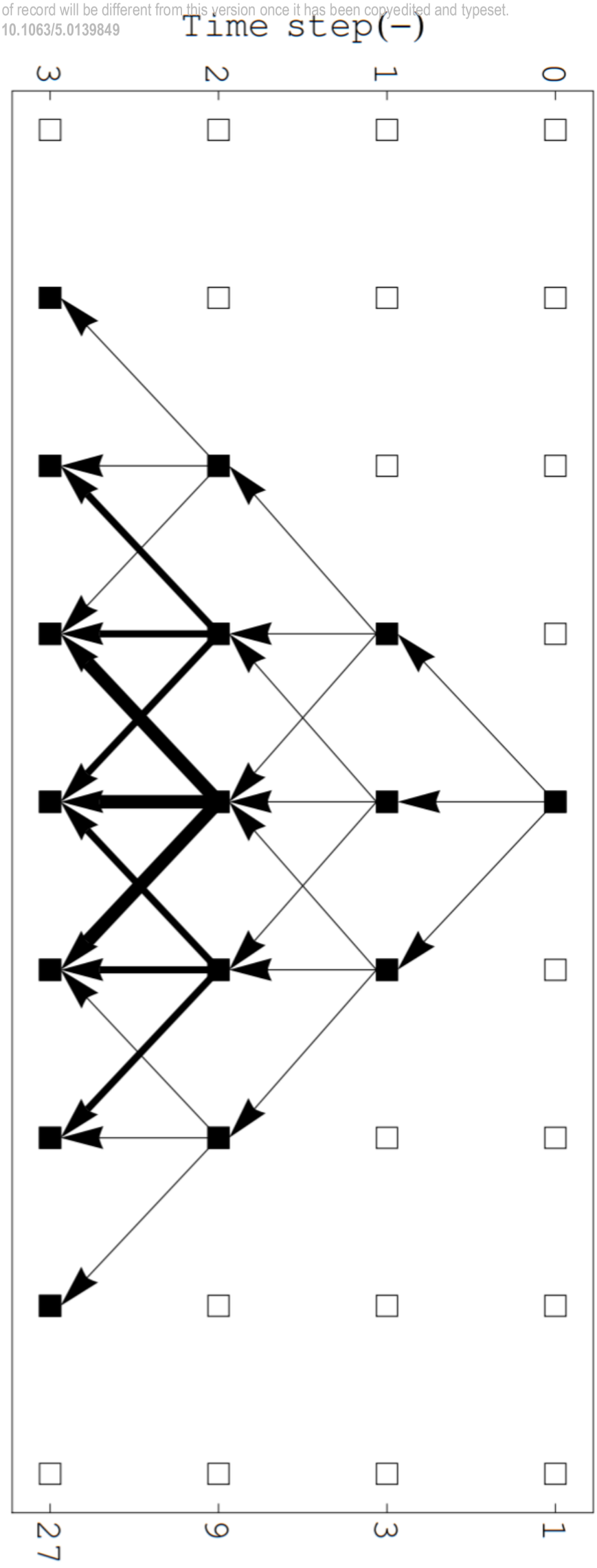

AIP Publishing

Chaos
An Interdisciplinary Journal
of Nonlinear Science

PLEASE CITE THIS ARTICLE AS DOI: 10.1063/5.0139849

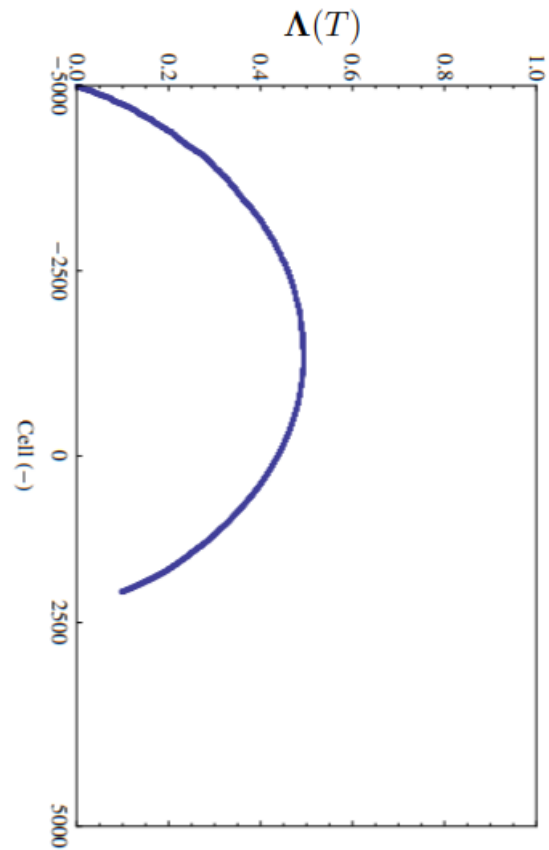

AIP Publishing

Chaos
An Interdisciplinary Journal
of Nonlinear Science

PLEASE CITE THIS ARTICLE AS DOI: 10.1063/5.0139849

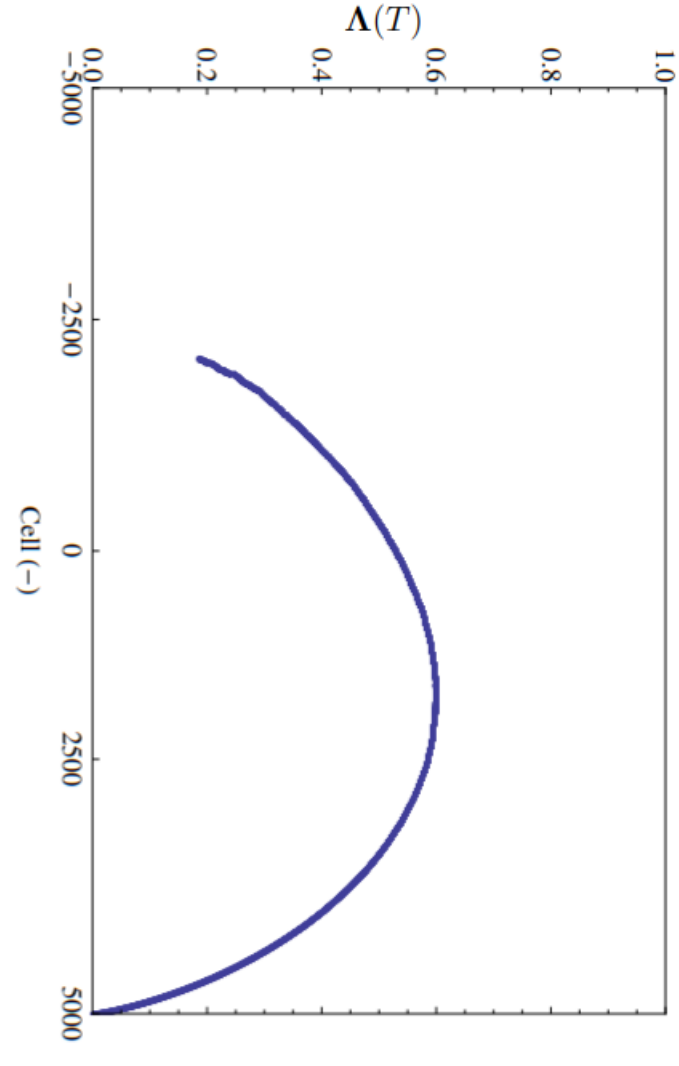

AIP Publishing

Chaos
An Interdisciplinary Journal
of Nonlinear Science

PLEASE CITE THIS ARTICLE AS DOI: 10.1063/5.0139849

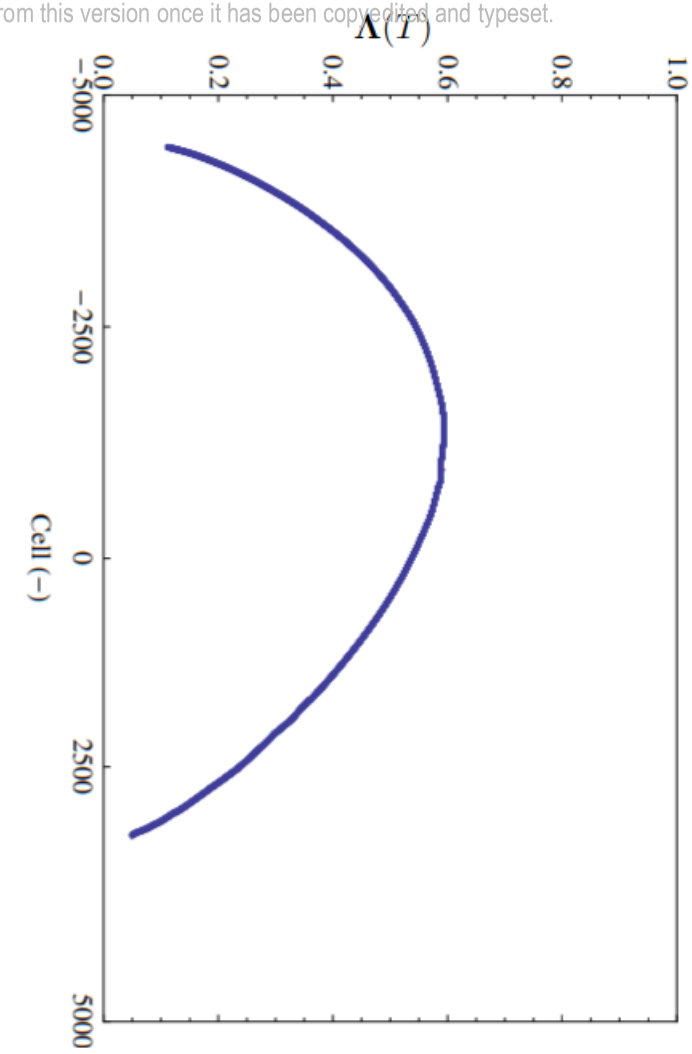

AIP Publishing

Chaos
An Interdisciplinary Journal
of Nonlinear Science

PLEASE CITE THIS ARTICLE AS DOI: 10.1063/5.0139849

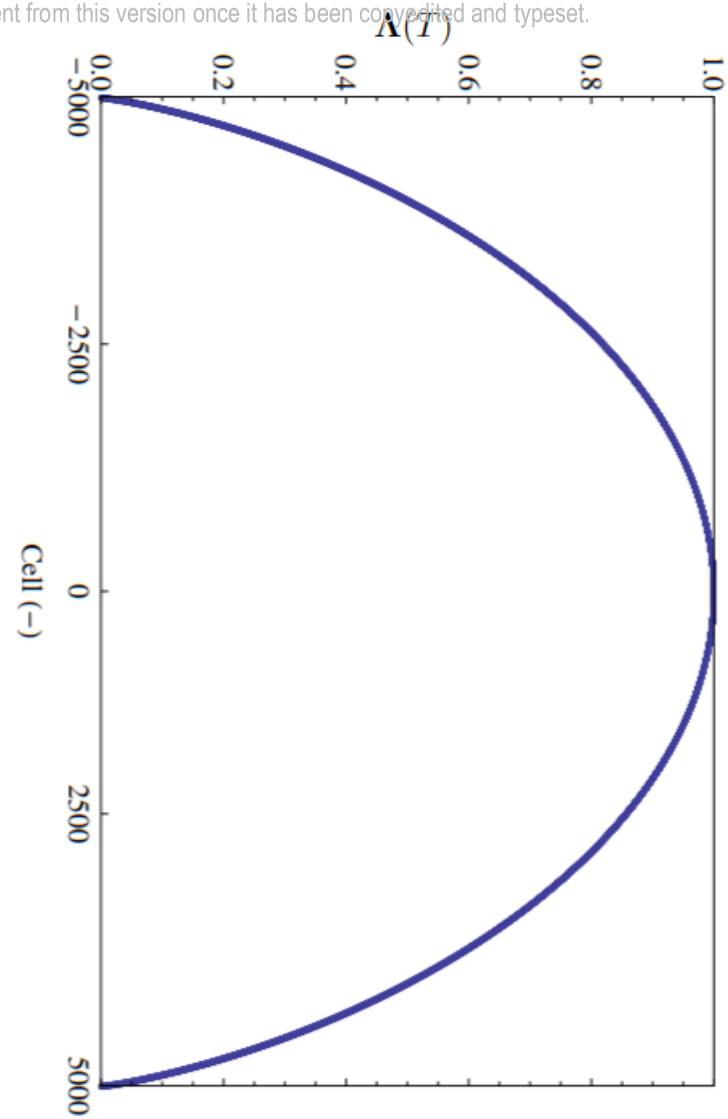

AIP Publishing

Chaos
An Interdisciplinary Journal
of Nonlinear Science

PLEASE CITE THIS ARTICLE AS DOI: 10.1063/5.0139849

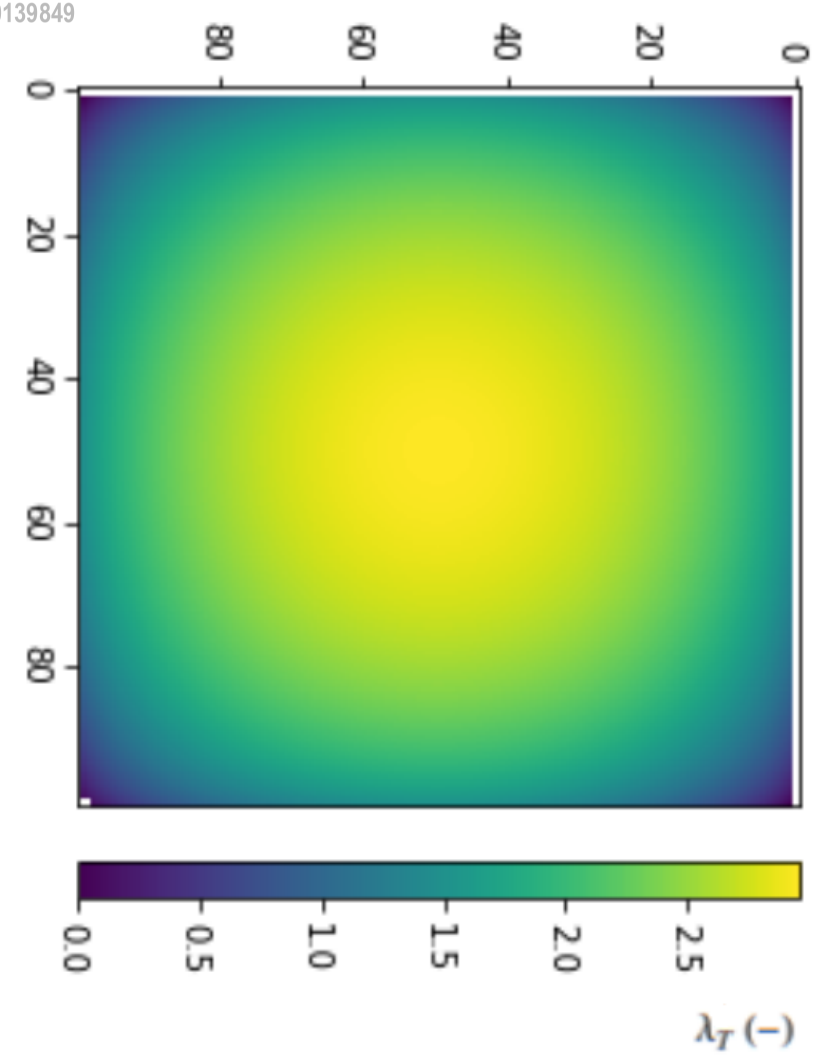

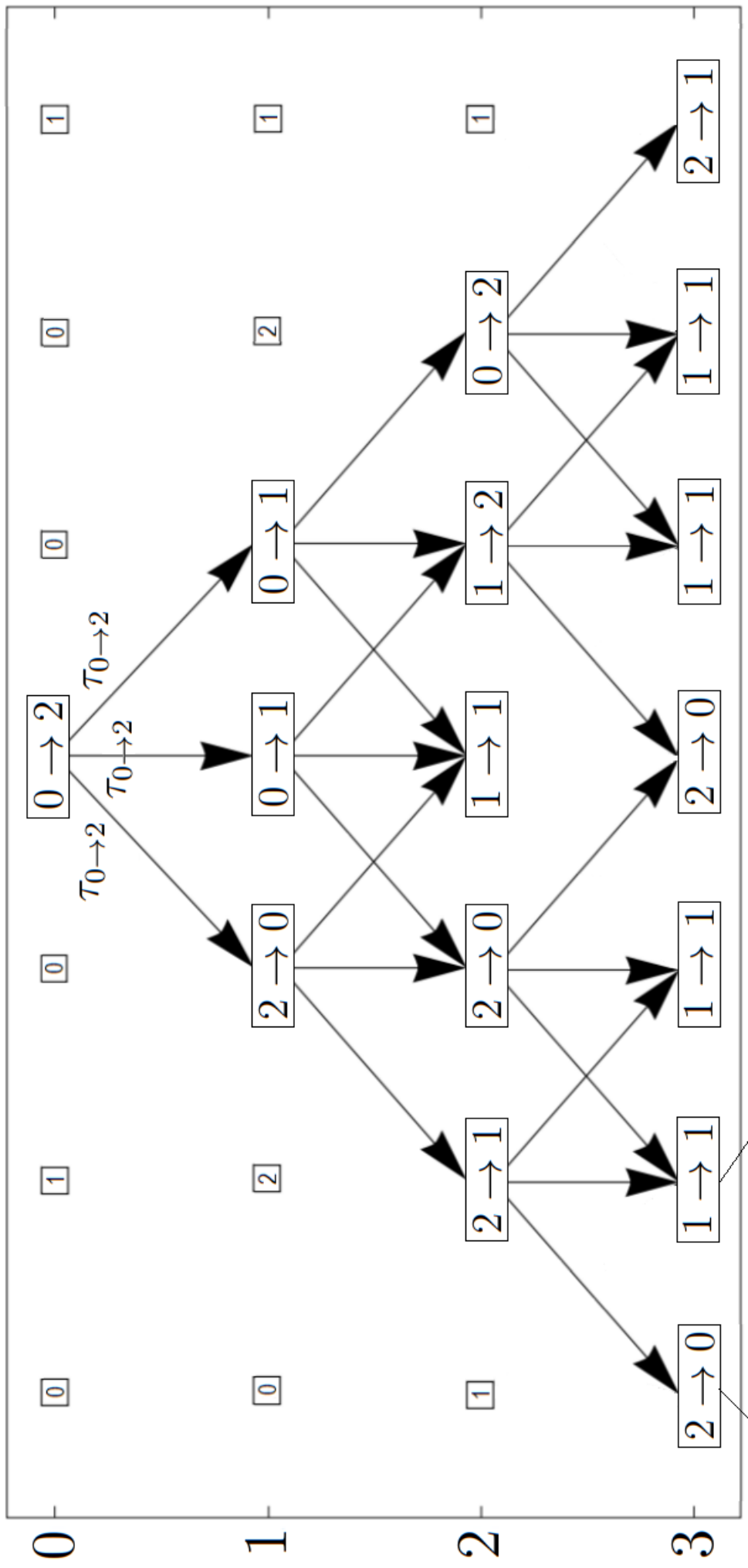

AIP Publishing

Chaos
An Interdisciplinary Journal
of Nonlinear Science

PLEASE CITE THIS ARTICLE AS DOI: 10.1063/5.0139849

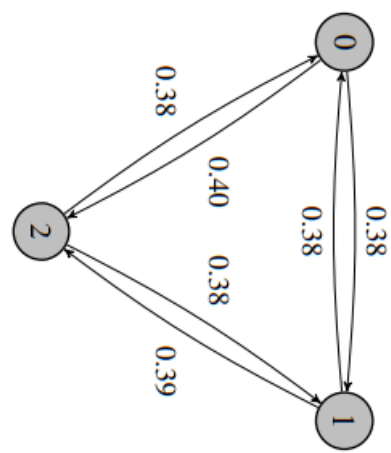

AIP Publishing

Chaos
An Interdisciplinary Journal
of Nonlinear Science

PLEASE CITE THIS ARTICLE AS DOI: 10.1063/5.0139849

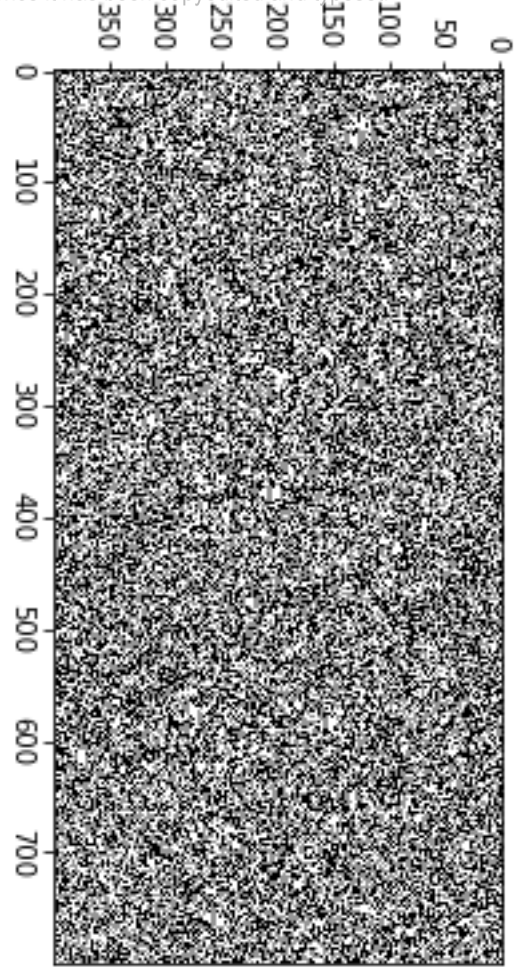

AIP Publishing

Chaos
An Interdisciplinary Journal
of Nonlinear Science

PLEASE CITE THIS ARTICLE AS DOI: 10.1063/5.0139849

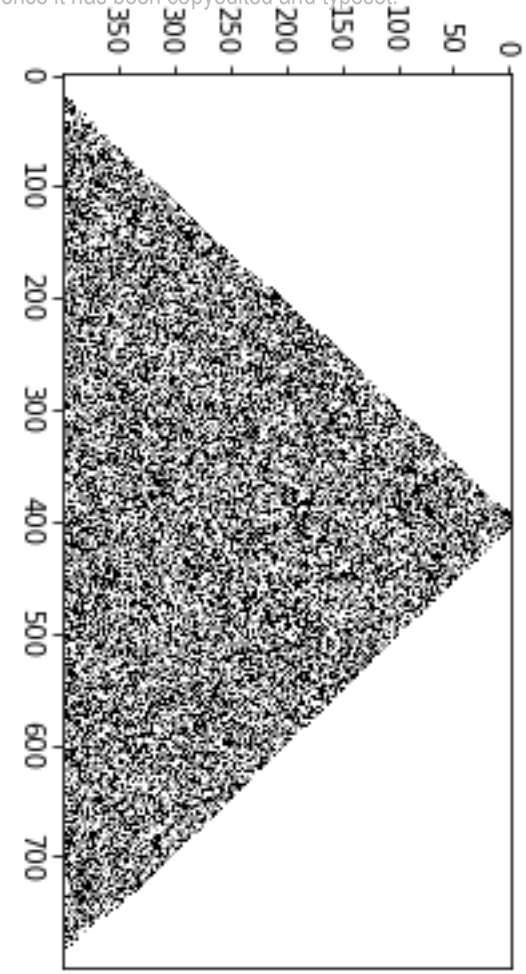

AIP Publishing

Chaos
An Interdisciplinary Journal
of Nonlinear Science

PLEASE CITE THIS ARTICLE AS DOI: 10.1063/5.0139849

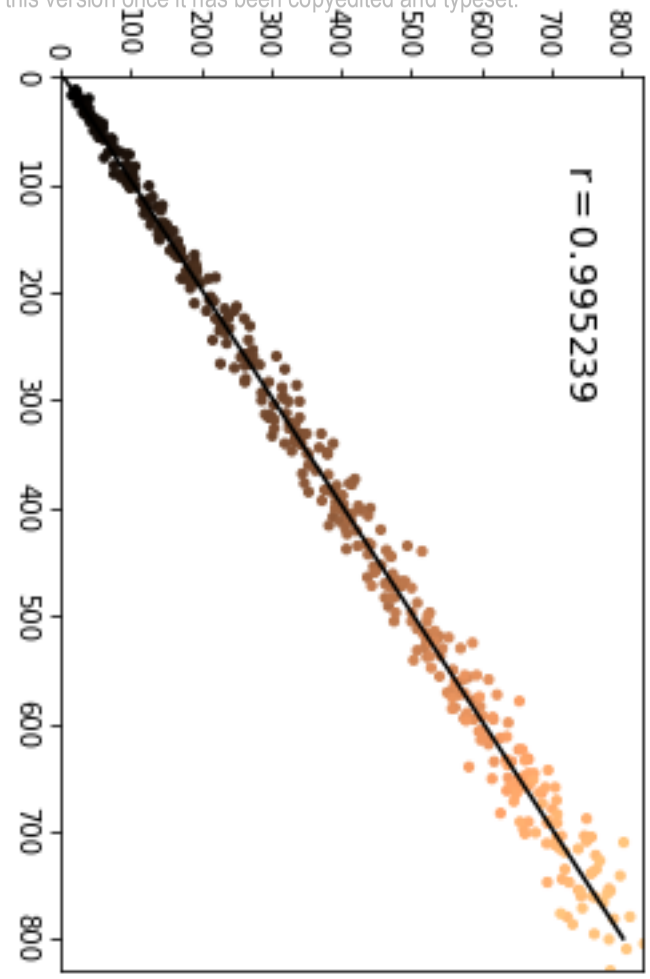

AIP Publishing

Chaos
An Interdisciplinary Journal
of Nonlinear Science

PLEASE CITE THIS ARTICLE AS DOI: 10.1063/5.0139849

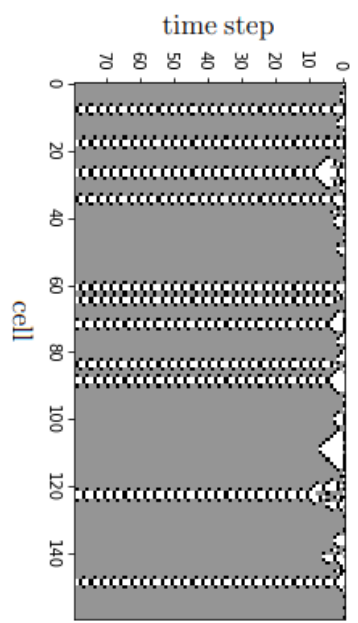

AIP Publishing

Chaos
An Interdisciplinary Journal
of Nonlinear Science

PLEASE CITE THIS ARTICLE AS DOI: 10.1063/5.0139849

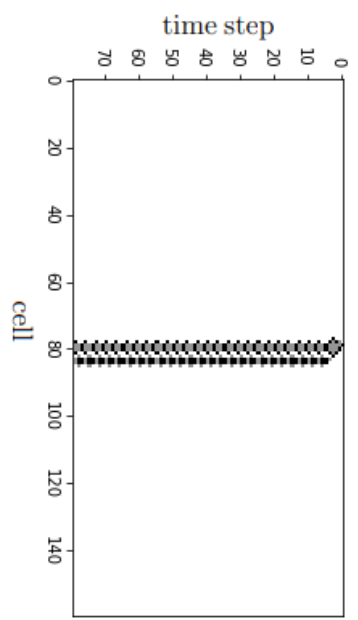

AIP Publishing

Chaos
An Interdisciplinary Journal
of Nonlinear Science

PLEASE CITE THIS ARTICLE AS DOI: 10.1063/5.0139849

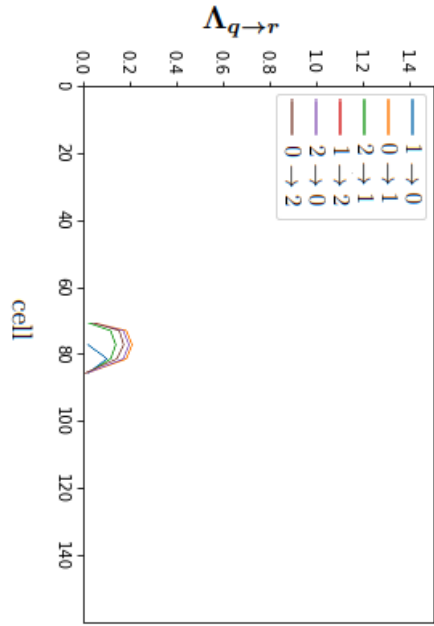

AIP Publishing

Chaos
An Interdisciplinary Journal
of Nonlinear Science

ACCEPTED MANUSCRIPT

PLEASE CITE THIS ARTICLE AS DOI: 10.1063/5.0139849

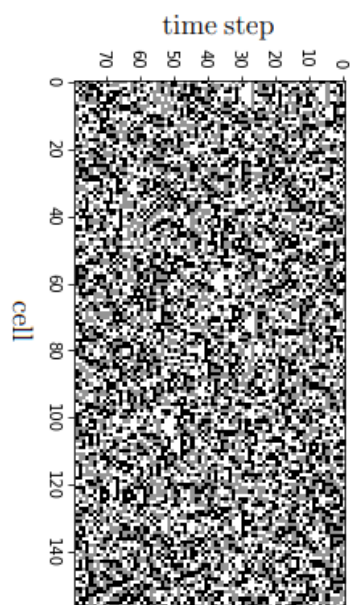

AIP Publishing

Chaos
An Interdisciplinary Journal
of Nonlinear Science

PLEASE CITE THIS ARTICLE AS DOI: 10.1063/5.0139849

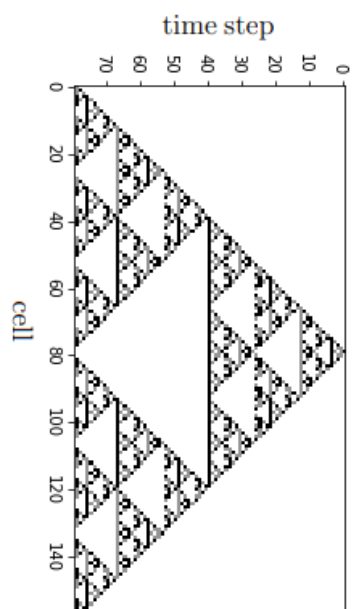

AIP Publishing

Chaos
An Interdisciplinary Journal
of Nonlinear Science

PLEASE CITE THIS ARTICLE AS DOI: 10.1063/5.0139849

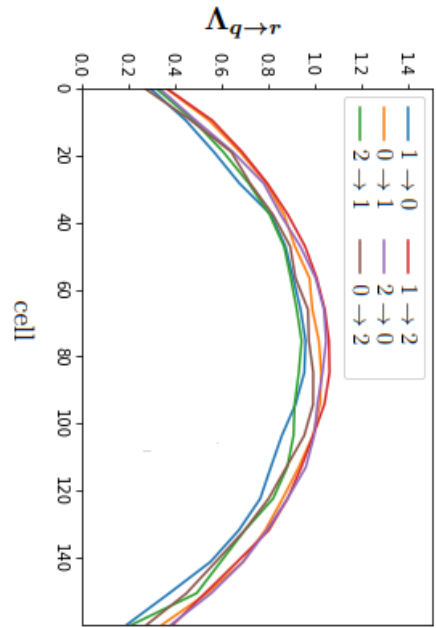

AIP Publishing

Chaos
An Interdisciplinary Journal
of Nonlinear Science

PLEASE CITE THIS ARTICLE AS DOI: 10.1063/5.0139849

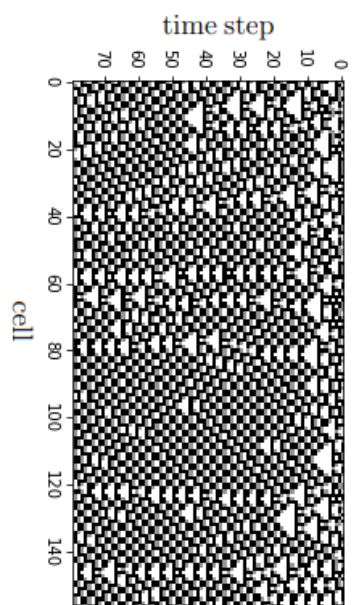

AIP Publishing

Chaos
An Interdisciplinary Journal
of Nonlinear Science

PLEASE CITE THIS ARTICLE AS DOI: 10.1063/5.0139849

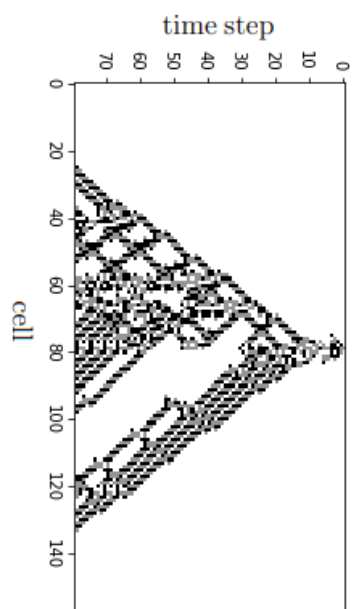

AIP Publishing

Chaos
An Interdisciplinary Journal
of Nonlinear Science

PLEASE CITE THIS ARTICLE AS DOI: 10.1063/5.0139849

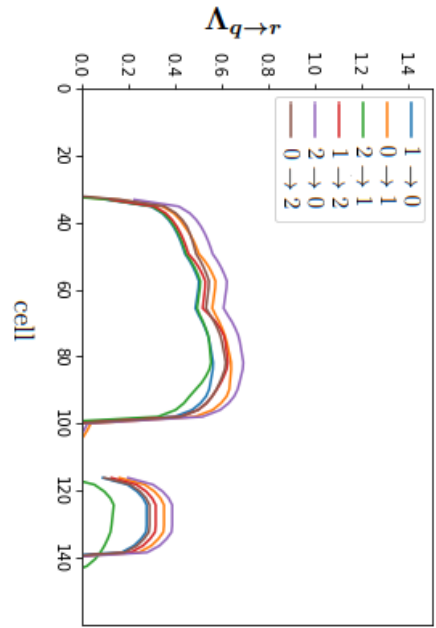

AIP Publishing

Chaos
An Interdisciplinary Journal
of Nonlinear Science

PLEASE CITE THIS ARTICLE AS DOI: 10.1063/5.0139849

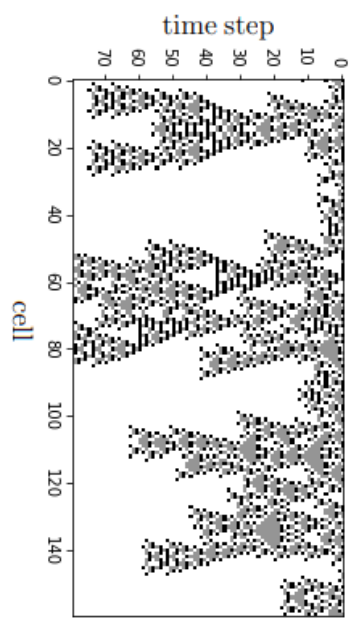

AIP Publishing

Chaos
An Interdisciplinary Journal
of Nonlinear Science

PLEASE CITE THIS ARTICLE AS DOI: 10.1063/5.0139849

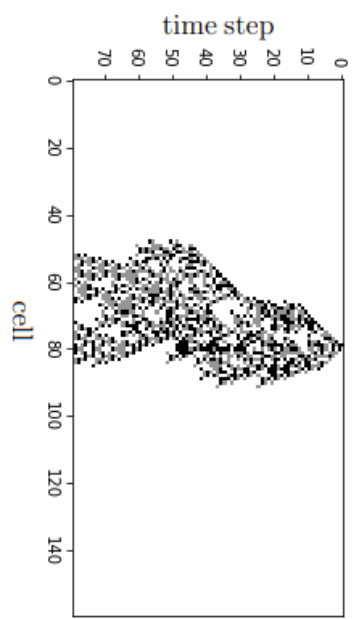

AIP Publishing

Chaos
An Interdisciplinary Journal
of Nonlinear Science

PLEASE CITE THIS ARTICLE AS DOI: 10.1063/5.0139849

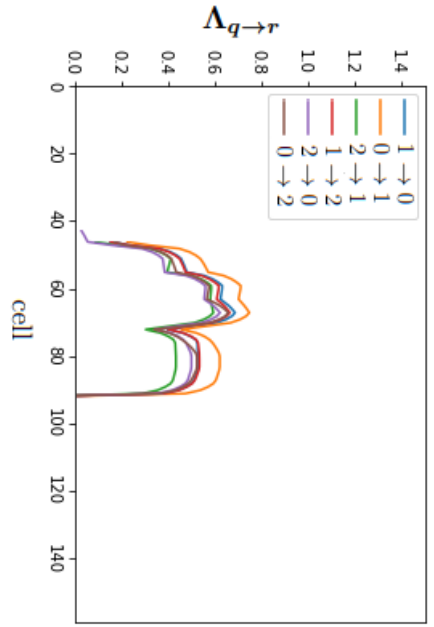

AIP Publishing

Chaos
An Interdisciplinary Journal
of Nonlinear Science

PLEASE CITE THIS ARTICLE AS DOI: 10.1063/5.0139849

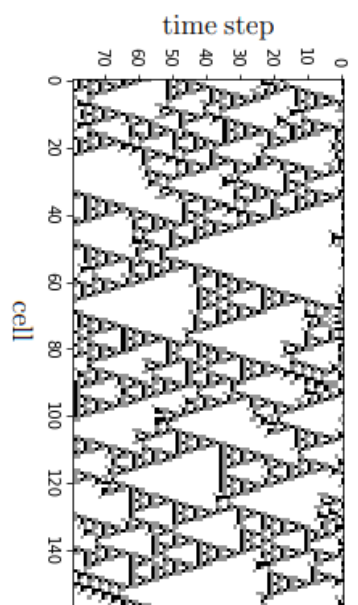

AIP Publishing

Chaos
An Interdisciplinary Journal
of Nonlinear Science

PLEASE CITE THIS ARTICLE AS DOI: 10.1063/5.0139849

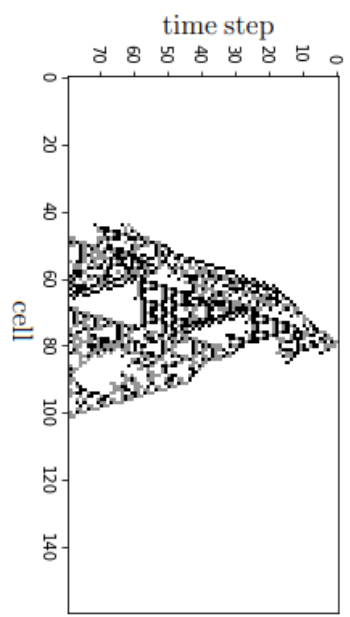

AIP Publishing

Chaos
An Interdisciplinary Journal
of Nonlinear Science

PLEASE CITE THIS ARTICLE AS DOI: 10.1063/5.0139849

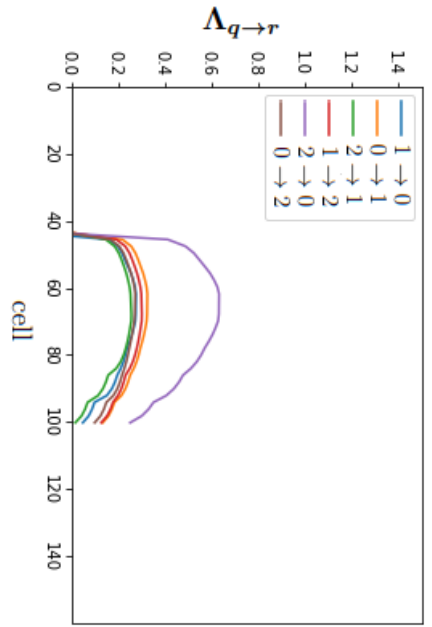

AIP Publishing

Chaos
An Interdisciplinary Journal
of Nonlinear Science

PLEASE CITE THIS ARTICLE AS DOI: 10.1063/5.0139849

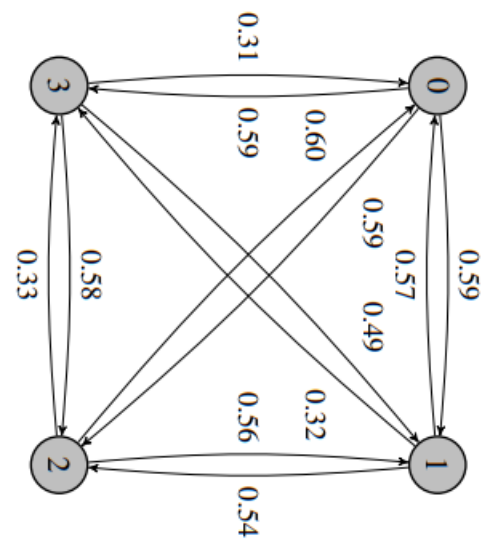

AIP Publishing

Chaos
An Interdisciplinary Journal
of Nonlinear Science

PLEASE CITE THIS ARTICLE AS DOI: 10.1063/5.0139849

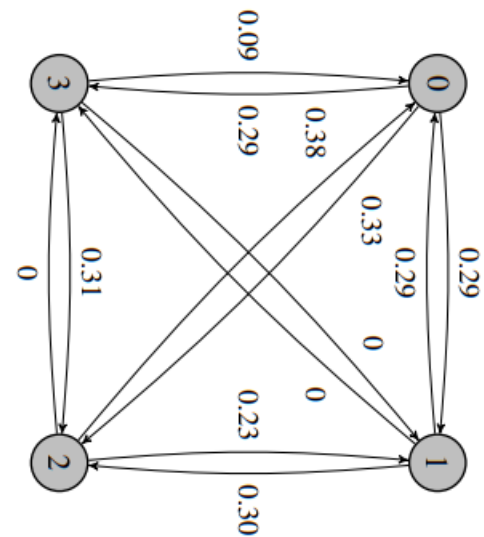

AIP Publishing

Chaos
An Interdisciplinary Journal
of Nonlinear Science

PLEASE CITE THIS ARTICLE AS DOI: 10.1063/5.0139849

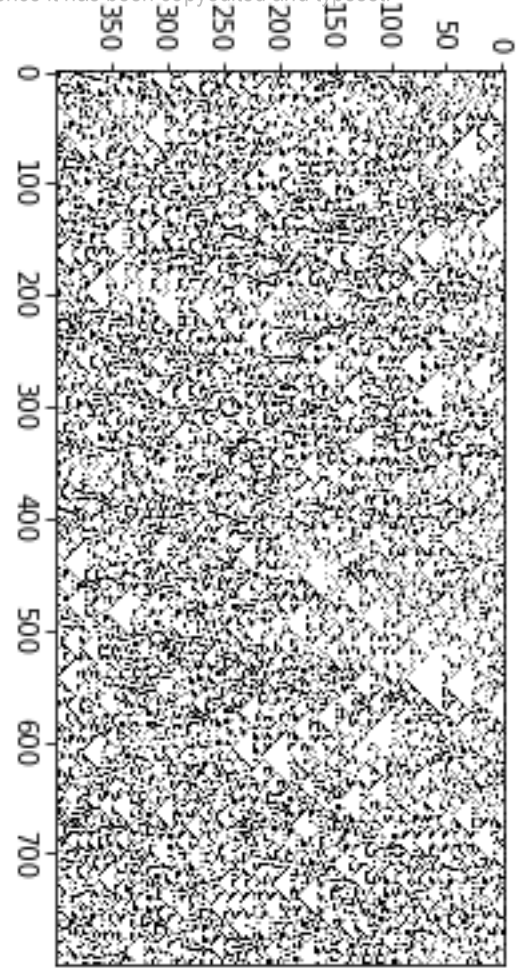

AIP Publishing

Chaos
An Interdisciplinary Journal
of Nonlinear Science

PLEASE CITE THIS ARTICLE AS DOI: 10.1063/5.0139849

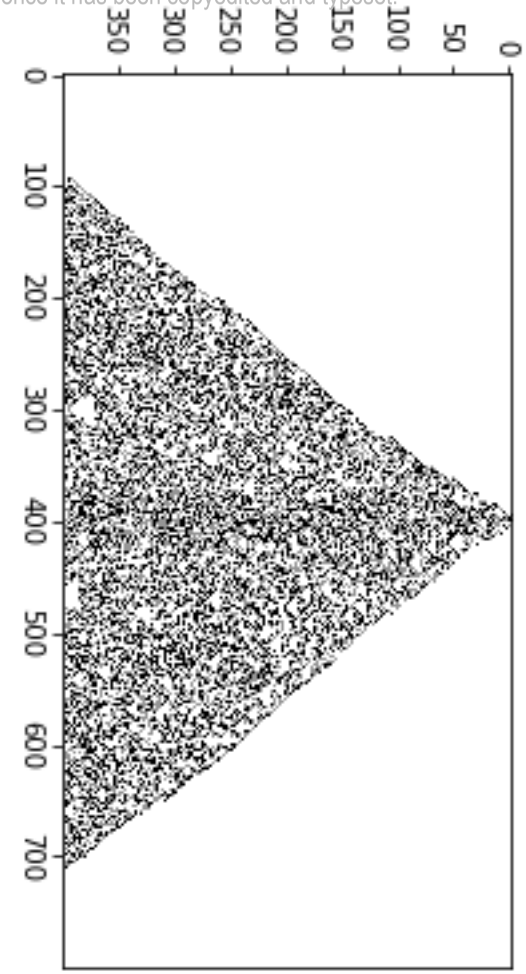

AIP Publishing

Chaos
An Interdisciplinary Journal
of Nonlinear Science

PLEASE CITE THIS ARTICLE AS DOI: 10.1063/5.0139849

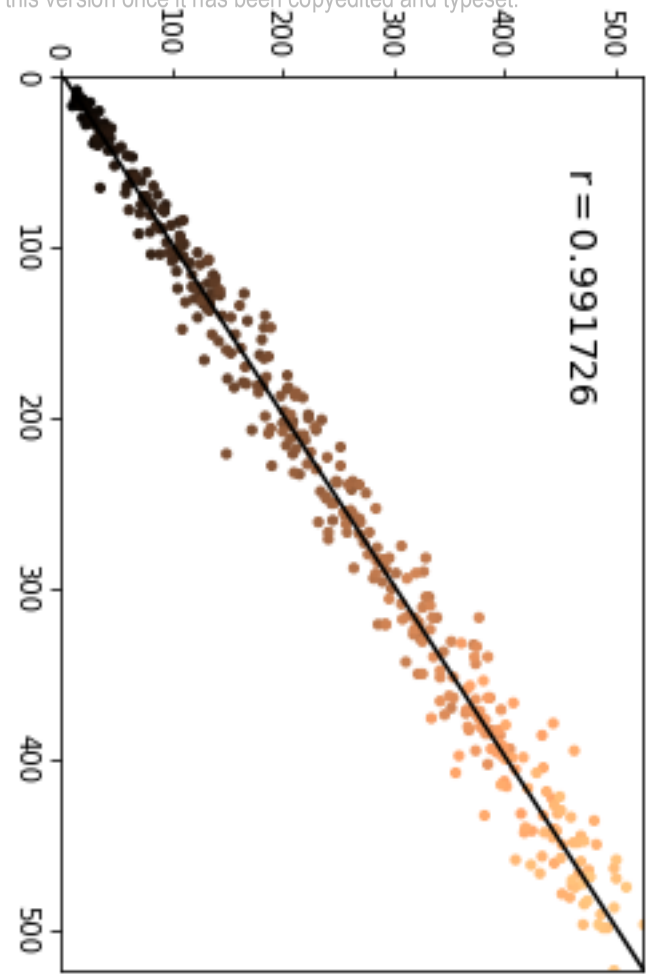

AIP Publishing

Chaos
An Interdisciplinary Journal
of Nonlinear Science

PLEASE CITE THIS ARTICLE AS DOI: 10.1063/5.0139849

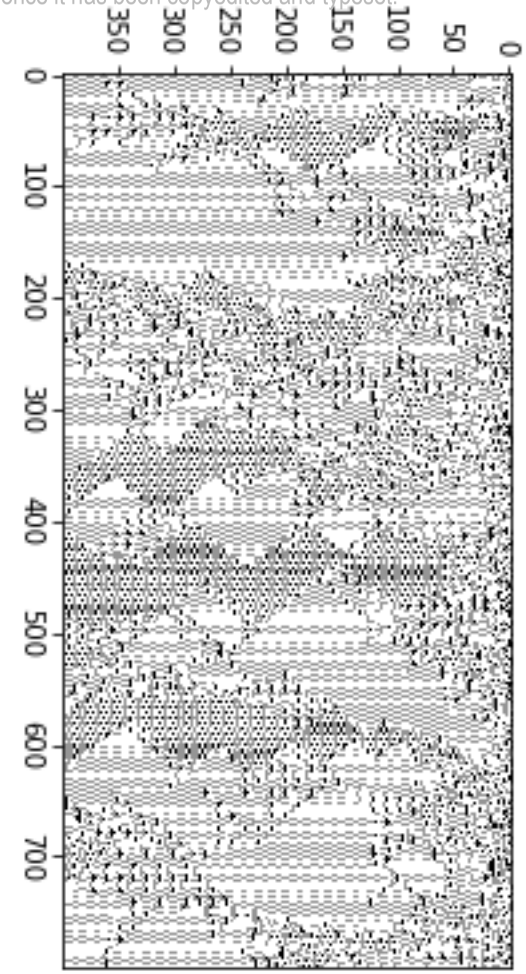

AIP Publishing

Chaos
An Interdisciplinary Journal
of Nonlinear Science

PLEASE CITE THIS ARTICLE AS DOI: 10.1063/5.0139849

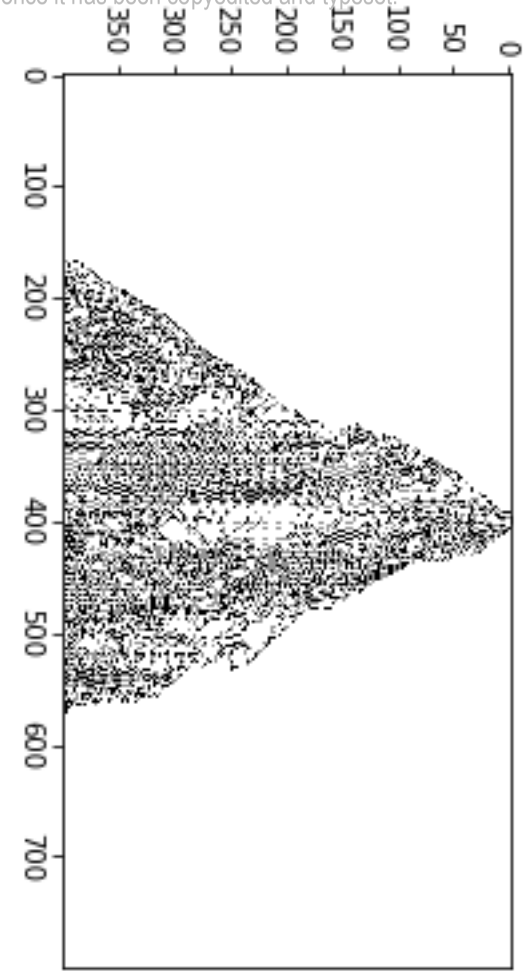

AIP Publishing

Chaos
An Interdisciplinary Journal
of Nonlinear Science

PLEASE CITE THIS ARTICLE AS DOI: 10.1063/5.0139849

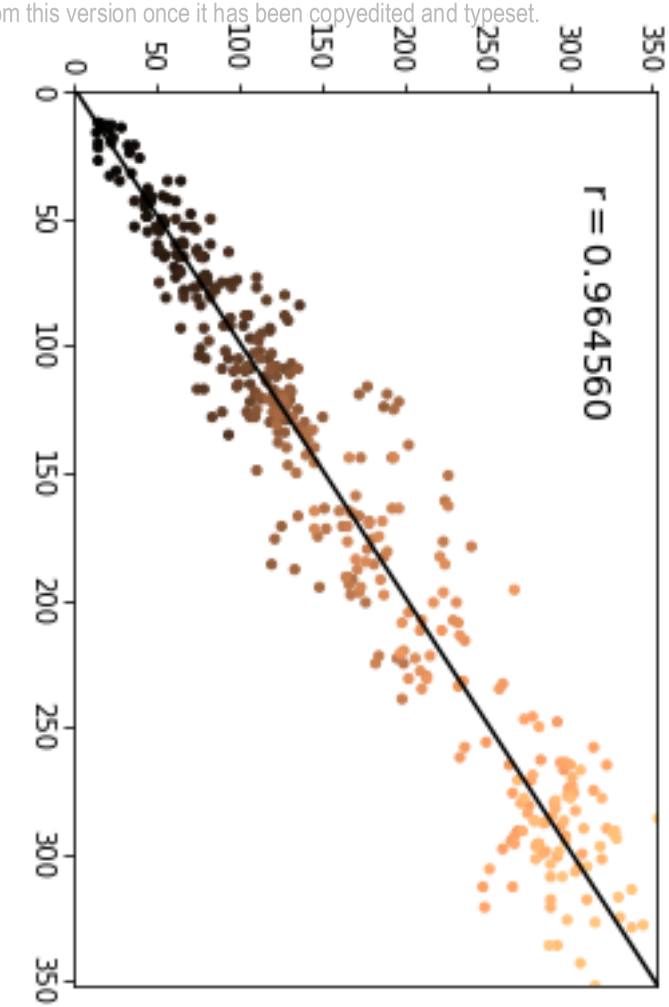

AIP Publishing

Chaos
An Interdisciplinary Journal
of Nonlinear Science

PLEASE CITE THIS ARTICLE AS DOI: 10.1063/5.0139849

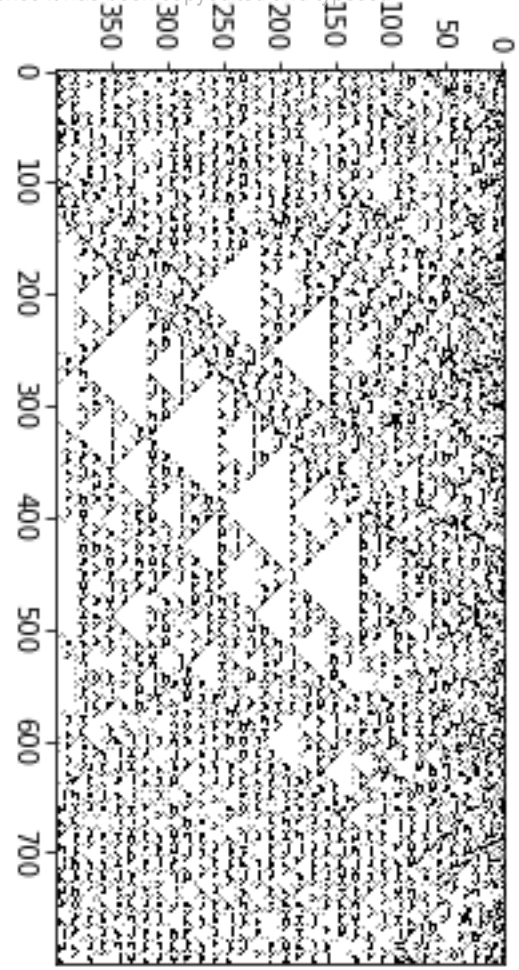

AIP Publishing

Chaos
An Interdisciplinary Journal
of Nonlinear Science

PLEASE CITE THIS ARTICLE AS DOI: 10.1063/5.0139849

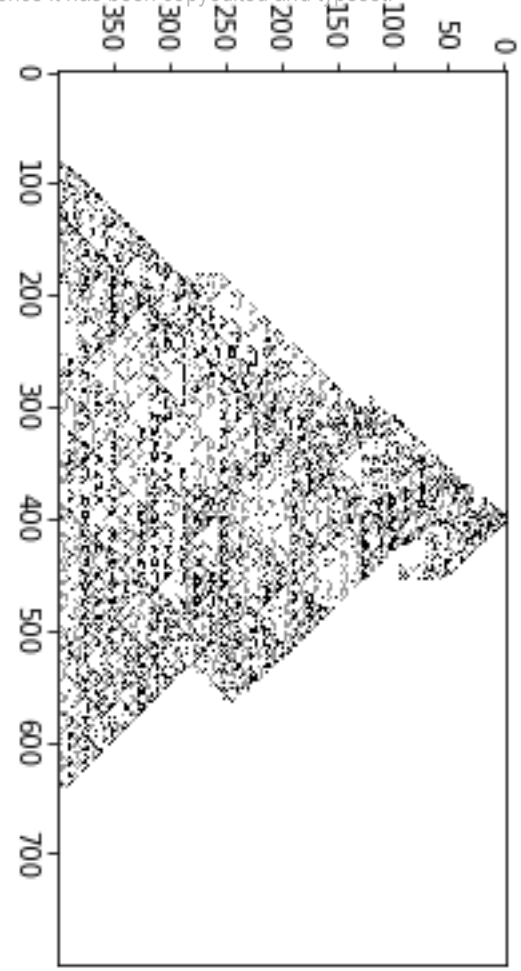

AIP Publishing

Chaos
An Interdisciplinary Journal
of Nonlinear Science

PLEASE CITE THIS ARTICLE AS DOI: 10.1063/5.0139849

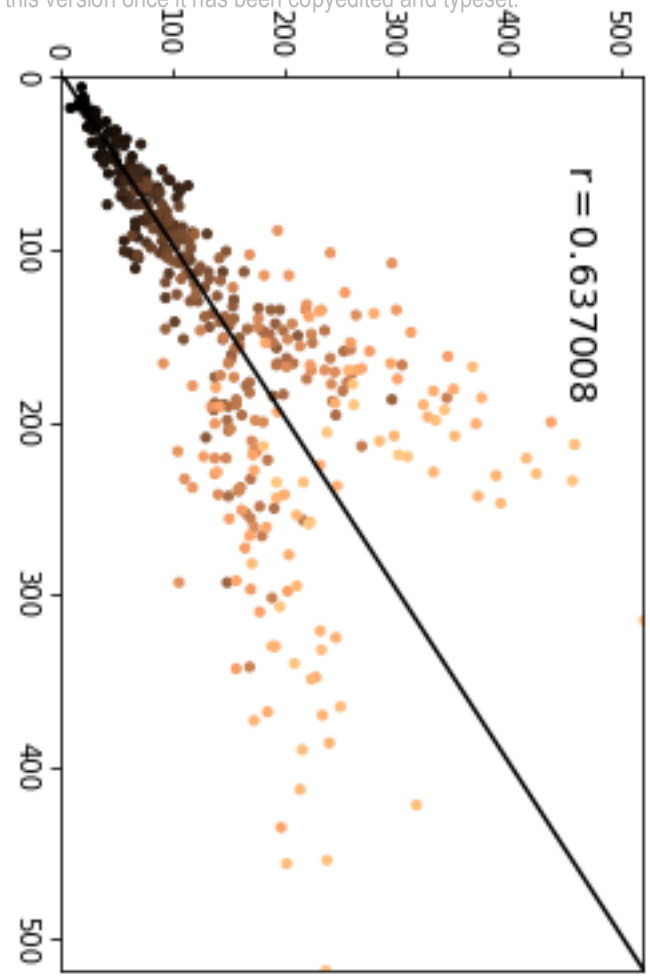

AIP Publishing

Chaos
An Interdisciplinary Journal
of Nonlinear Science

PLEASE CITE THIS ARTICLE AS DOI: 10.1063/5.0139849

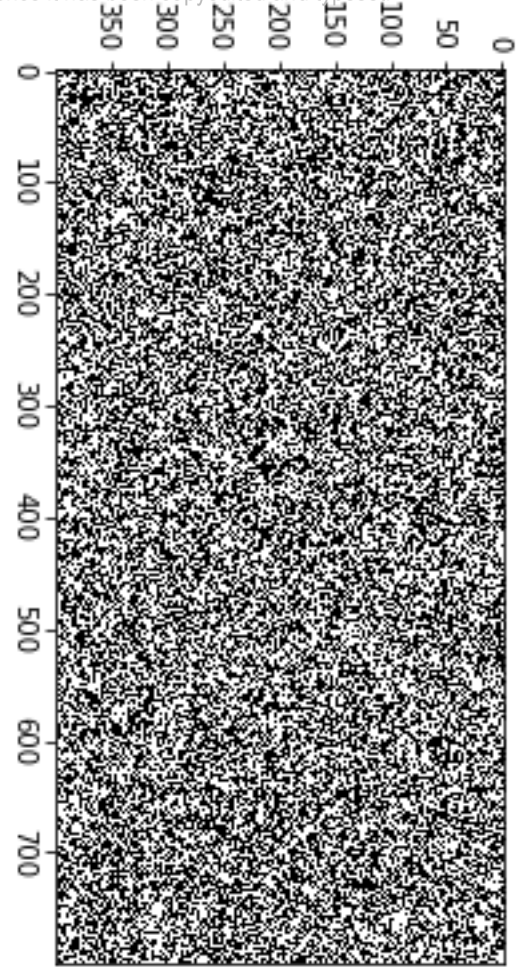

AIP Publishing

Chaos
An Interdisciplinary Journal
of Nonlinear Science

PLEASE CITE THIS ARTICLE AS DOI: 10.1063/5.0139849

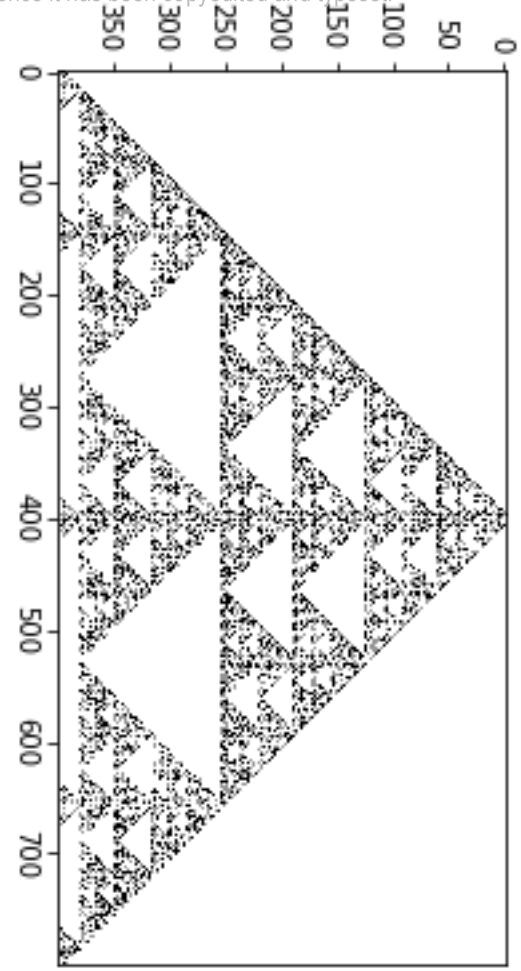

AIP Publishing

Chaos
An Interdisciplinary Journal
of Nonlinear Science

PLEASE CITE THIS ARTICLE AS DOI: 10.1063/5.0139849

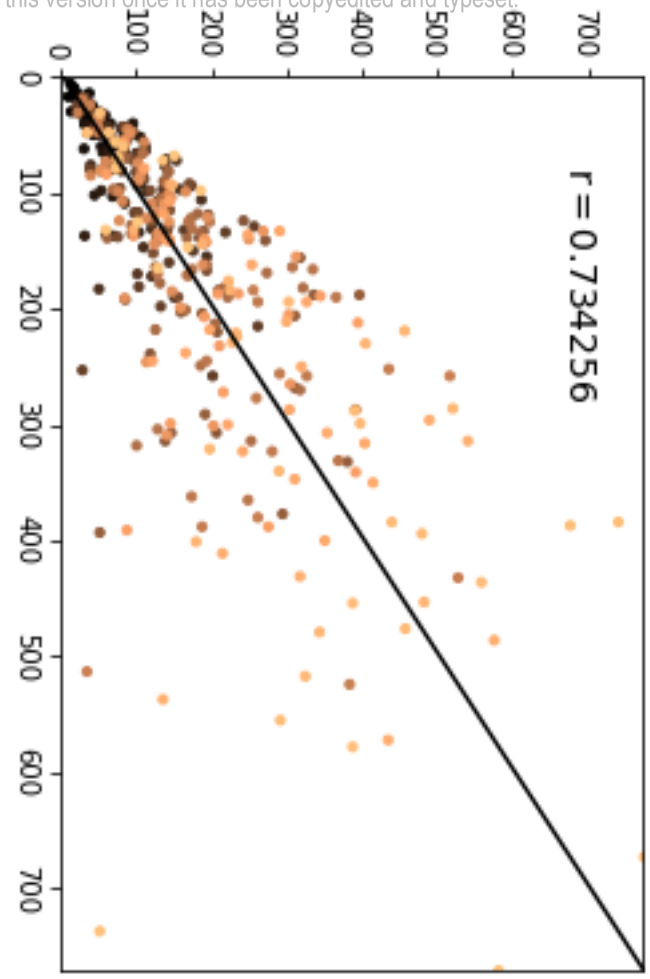

AIP Publishing

Chaos
An Interdisciplinary Journal
of Nonlinear Science

PLEASE CITE THIS ARTICLE AS DOI: 10.1063/5.0139849

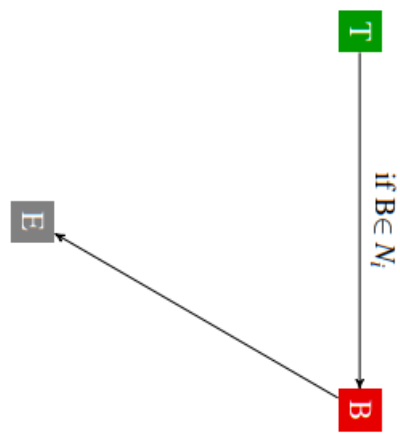

AIP Publishing

Chaos
An Interdisciplinary Journal
of Nonlinear Science

PLEASE CITE THIS ARTICLE AS DOI: 10.1063/5.0139849

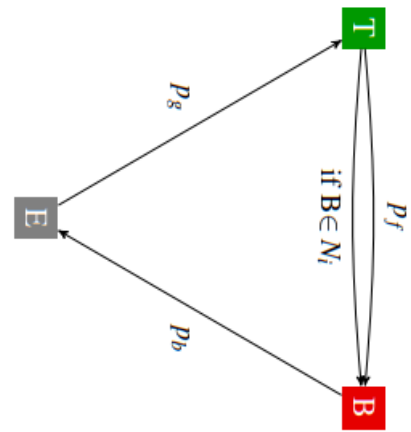

Chaos
An Interdisciplinary Journal
of Nonlinear Science

AIP Publishing

Chaos
An Interdisciplinary Journal
of Nonlinear Science

AIP Publishing